Kruhl, J. H., Griesshaber, E., Schmahl, W. W., Wirth, R. (2024): Fracturing and widening of grain boundary networks in quartz, plagioclase and olivine crystal aggregates during exhumation at low P-T conditions. - Journal of Structural Geology, 179, 105032.

https://doi.org/10.1016/j.jsg.2023.105032

Fracturing and widening of grain boundary networks in quartz, plagioclase and olivine crystal aggregates during exhumation at low P-T conditions

Jörn H. Kruhl[a*], Erika Griesshaber[a], Wolfgang W. Schmahl[a], Richard Wirth[b]

[a] Department of Earth and Environmental Sciences, Ludwig-Maximilians-Universität, 80333 Munich, Germany

[b] Helmholtz Centre Potsdam, GFZ German Research Centre for Geosciences, Potsdam, Germany

* Corresponding author, +498921804351

Jörn H. Kruhl	kruhl@tum.de
Erika Griesshaber	e.griesshaber@lrz.uni-muenchen.de
Wolfgang W. Schmahl	Wolfgang.W.Schmahl@lrz.uni-muenchen.de
Richard Wirth	wirth@gfz-potsdam.de

Abstract

Grain boundary networks of quartz, plagioclase and olivine crystal aggregates in metamorphic rocks have been investigated from the nanometer to the millimeter scale by polarized-light microscopy, SEM, and TEM. The studied materials show different grain sizes and experienced different retrograde P-T histories. The aggregates of quartz and plagioclase are traversed by networks of ~90% continuously open boundaries with µm-sized cavities along the boundaries or at triple junctions. The boundaries are up to ~500 nm wide open with typically parallel opposing grain faces. Olivine boundaries are filled with serpentine that does not replace olivine but fills the initially open space homogeneously and mostly with random orientation. For quartz there is no correlation between the crystallographic orientation of grain boundaries and their widths. Amongst all samples analyzed, a weak positive correlation exists between grain size and width of open grain boundaries. The application of measured volume changes and elasticity data from the literature to the cooling-decompression paths of the analyzed materials suggests that fracturing with subsequent widening of the grain boundaries starts at temperatures recognizably below the transition from crystal-plastic to brittle behavior of quartz, plagioclase and olivine but not only under surface conditions. The high

amount of open boundaries causes an extensive permeability.

Keywords

Open grain boundaries, SEM, TEM, quartz, plagioclase, olivine

1. Introduction

Grain and phase boundaries strongly influence physical properties of crystalline materials; such as strength, rheological behavior, resistance to corrosion, reactivity, conductivity, or permeability (Behrmann, 1985; Mainprice et al., 1993; Aust et al., 1994; Shimada et al., 2002; Frary and Schuh, 2005, and references therein; Nagurney et al., 2021; Freitag et al., 2022). They affect a variety of processes as for instance deformation, metamorphic reactions, metasomatism or weathering (Voll, 1960; White and White, 1981; Yardley, 1989; Delvigne, 1998; Mancktelow and Pennacchioni, 2004; Vernon, 2004; Bukovská et al., 2015). Although grain and phase boundaries are regarded as generally closed structures, early transmission electron microscopy (TEM) mostly on quartz illustrated voids and open sections along boundaries in crystal aggregates but could not address this phenomenon in depth, due to the limitations of instruments available at that time (White, 1976; Doukhan and Trepied, 1979; Bell and Wilson, 1981; Behrmann, 1985; Watson and Brenan, 1987; Hippertt, 1994; Hiraga et al., 1999; Duyster and Stöckhert, 2001). More recent scanning electron microscopy (SEM) and TEM on natural as well as experimentally treated material, the former mostly on broken surfaces of crystal aggregates, revealed the existence of nanometer-sized voids and open sections along grain boundaries and of tubular voids with crystallographically controlled 3D shapes along three-grains junctions (Mancktelow et al., 1998; Mancktelow and Pennacchioni, 2004; Schenk and Urai, 2004; Price et al., 2006; Schenk et al., 2006; Fusseis et al., 2009; Schmatz and Urai, 2011; Billia et al., 2013; Burnard et al., 2015; Freitag et al., 2022).

Recent TEM studies show that grain boundaries of quartz (Qz) and calcite (Cal) as well as phase boundaries of feldspars (Fsp), amphiboles (Amp), orthopyroxene (Opx) and clinopyroxenes (Cpx) (abbreviations of mineral names after Whitney and Evans, 2010) in metamorphic and magmatic rocks are generally several hundred nanometers wide and completely open or partly filled with secondary low-T minerals (Kruhl et al., 2013; Wirth et al., 2021). These investigations also hint at permeability of grain boundary networks in 3D and propose volume reduction due to cooling and decompression during exhumation as mechanism of cracking and widening of grain and phase boundaries. Recent SEM studies on Qz grain boundaries provide supporting data (Nagurney et al., 2021). However, the amount of available data is still very small and currently supplemented by numerical modelling only to a limited extend (Raghami et al., 2020). Consequently, the cracking and widening mechanism is not well understood and the question is not answered at which P-T-conditions grain and phase boundaries fracture, open and form connected networks that cause permeability for fluids on a larger scale. The answers will deepen our knowledge about physical properties of crystalline materials at surface conditions and different depths of the continental and oceanic crust. Beyond that, the answers will shape our views on various geological processes, such as weathering, fluid transport, reactivity, and behavior of crystalline material under different deformation conditions in nature and experiments.

Due to the high resolution methods required, the previous studies all examined only a small number of instances, and thus, statistically sound data sets on size, frequency and distribution of voids are missing, with few exceptions (Schmatz and Urai, 2011; Billia et al., 2013). The same is true for geometry, size and crystallographic orientation of open or partly open grain and phase boundaries. Therefore, knowledge about the origin, properties, occurrence and significance of these micro-scale fabrics is still limited.

Local observations and limited data sets always leave some doubt about the statistical significance of an observation and the validity of more general conclusions. Therefore, with the present work, using high-resolution SEM with additional polarized-light microscopy, we access larger data sets, cover larger volumes and observe open grain and phase boundaries and their connectivity on a larger scale. Our study objects are grain boundaries of quartz, plagioclase and olivine – all minerals with strongly anisotropic, well-known thermo-elastic properties. The analyzed samples experienced different maximum P-T conditions and different exhumation P-T paths, and contain a wide range of grain sizes. This allows investigating the effects of microfabrics and P-T variations on cracking and widening of grain boundaries.

2. Methods

Our investigations are based on polarized-light and Scanning Electron Microscopy (SEM). In addition, Transmission Electron Microscopy (TEM) was applied, based on focused ion beam (FIB) sample preparation. Crystallographic orientations of grains and grain boundaries were determined by universal stage and grain areas were measured on the basis of digitized grain boundaries and with the aid of the open source image analysis program *ImageJ* (https://imagej.net/).

TEM was carried out with a Tecnai F20 X- twin electron microscope with a Schottky field emitter as electron source and equipped with a Gatan Tridiem Imaging Filter GIF, a Fishione high-angle annular dark field (HAADF) detector operating at a camera length (330 mm), which allows Z-contrast plus diffraction contrast imaging, and an EDAX X-Ray analyzer. EDX analyses were performed in scanning transmission mode (STEM) to prevent beam damage. Typically, acquisition time was 60 s and bright field images were acquired as energy filtered images applying a 20 eV window to the zero loss peak. For Qz at lower magnification, images were generally acquired in the scanning transmission mode as HAADF images, thus reducing the irradiation damage considerably. FIB sample preparation (Wirth, 2009) does not produce any of the grain boundary features described in our study. This was already discussed in previous papers (Kruhl et al., 2013; Wirth et al., 2021) and is additionally based on the experience of more than 8,000 TEM foils sputtered with FIB from different materials and studied with TEM by one of the authors (RW).

Secondary electron and back scattered electron imaging was carried out on a Hitachi SU5000 field emission SEM. Thin section surfaces were coated with up to 12 nm of carbon or/and up to 8 nm of Pt/Pd.

Both TEM and SEM have advantages and disadvantages with respect to measuring open grain boundaries. In our investigations, TEM foils are cut perpendicular to planar grain boundary segments. Therefore, measured grain boundary thicknesses are not biased by observation geometry. Open boundaries of up to 15 nm width can be measured without problems (Wirth et al., 2021). Outbreaks or depressions around boundaries at the thin-section surface, due to grinding and polishing, are clearly visible (Fig. 1a, c) and do not affect the thickness measurements. On the basis of repeated measurements, the inaccuracy of measurements is estimated as only 5 nm (Wirth et al., 2021). On the other hand, the high effort of sample preparation and the small sizes of the foils (generally not larger than ca. 9 x 8 µm) strongly limit the amount of investigated material. The total length of grain and phase boundaries, recently studied and published (Kruhl et al., 2013; Wirth et al., 2021) adds up to ~600 µm.

In contrast, SEM can be applied to areas of thin-section size allowing measurement of a much higher number of grain boundaries and permitting investigation of grain boundary networks. Sample preparation requires comparatively low effort, although polishing needs caution. However, the accuracy of measurement is lower compared to TEM. (i) Boundaries are partly oblique to the thin-section surface and may show irregular margins. The cut-effect requires time-consuming corrections by measuring the inclinations of the grain boundaries, preferentially with the universal-stage. (ii) Fractures in the grain boundary network may lead to widening of boundaries and cause additional bias of the measured widths (Fig. 2). Such boundaries were not included in the measurements. Fractures can be recognized by two characteristics: They are clearly wider than the surrounding open boundaries and they may locally transect grains, as shown in figure 2. (iii) In contrast to TEM, grinding and polishing of the thin-section surface may lead to excavation of material at the open grain boundary down to a few µm, or to the rotation of µm-sized fragments into the open boundary. The frequency is controlled by the quality of grinding and polishing. Such excavations or fragments are only visible with larger magnifications and sharp images (Fig. 1b, d). They may bias the data by enlarging or reducing the widths of open grain boundaries measured at the thin-section surface. It can be excluded that the voids formed due to volume change during uplift. Firstly, there is a clear correlation with the quality of grinding and polishing. Secondly, the voids show curved surfaces typical for fracturing of quartz and are often closely related to fractures running away from the grain boundary. Thirdly, they can be never observed in TEM foils away from the thin section surface. Fourthly, cooling and decompression lead to gross volume reduction. Under such conditions there is no process or stress field imaginable, which could cause such voids.

It is also worth noting that the likelihood of such modification of the grain boundary width by grinding and polishing means that methods that probe the outer material topography, such as atomic force microscopy (AFM), can over- or underestimate the widths of open grain boundaries. In fact, each method that can be applied to study open grain boundaries has its own advantages and disadvantages in resolution, preparation artefacts and methodical bias of data, and thus it is advisable to apply different methods and obtain large datasets.

In general, measurements at lower magnifications – e.g. below a few thousand, depending on the quality of the image – may lead to overestimation of grain boundary widths. However, even at magnifications below 1,000 strongly oblique but open boundaries can be identified as open (Fig. 2b). With magnifications up to 10,000—50,000, as applied in our investigation, opening widths of boundaries not too strongly inclined, i.e. with angles against the thin section of more than 60-70°, can be measured down to ca. 20 nm.

We would like to point out that the measured width of an open or partially filled grain boundary does not necessarily represent the distance, by which the two opposite grains were shifted away from each other. This is illustrated best by TEM images of kinked boundaries (Fig. 3; Kruhl et al., 2013 – figure 4a; Wirth et al., 2021 – figure 1b). Without kinks the direction of opening in 2D cannot be determined with certainty. Consequently, all boundary widths, measured at TEM or SEM images, represent the component of displacement normal to the boundary.

The areas of investigation were selected in thin sections under the polarized-light microscope. Based on photomicrographs of these regions – with crossed polarizers and gypsum test plate for better differentiation – grains and grain boundaries were numbered and their coordinates determined. SEM images of boundaries and boundary networks were taken and the boundary widths determined directly in these images. The c-axes of neighboring Qz grains were measured with the aid of the universal stage together with the inclinations of grain boundaries against the thin section in order to correct the cut-effect. Grain areas were determined with the open source image analysis program *ImageJ*, based on digitized outlines of grains in photomicrographs. In this way, opening widths of grain boundaries could be related to areas and crystallographic orientations of neighboring grains. However, area measurements performed in 2D cuts through 3D grains lead to underestimation of grain sizes on a statistical basis. This has to be kept in mind when correlating grain size to other parameters, such as grain boundary width.

In total, widths of 604 grain boundaries were measured by SEM together with the adjoining grains (Tab. 1) at magnifications of generally 10,000 to 25,000, in certain cases up to 50,000. In each thin section the measured area of Qz and Pl aggregates covers several mm^2. Measurements on Ol cover the entire thin section, i.e., areas of ~1.5 cm^2. On a statistical basis, widths of open grain boundaries additionally measured with TEM in the same samples are in the same range as widths measured by SEM (Fig. 4).

3. Materials

Three minerals in eight samples and thirteen thin sections were analyzed by scanning and transmission electron microscopy (SEM and TEM): Qz in five samples, Pl in two samples, and Ol in one sample. The materials have different microfabrics and experienced a variation of exhumation P-T histories, covering greenschist to granulite facies conditions, contact and ultra-high-pressure metamorphism.

Sample HH147B is a deformed Qz vein from the Orune Schists of the late Variscan basement in eastern Sardinia (Italy). It consists of elongate, intensely deformed Qz grains with strong subgrain pattern and deep-lobate boundaries (Fig. 5a). These grains form new, small recrystallized grains. The vein is transected by late, open fractures. Maximum conditions of metamorphism of ~450-500 °C and ~0.55 GPa were followed by cooling and decompression (Helbing, 2003 – figures 5-3 and 5-12). These P-T conditions represent an average for the Orune Schists. The studied sample was collected from the southernmost, that is, upper part of the unit. Therefore, P-T conditions of ~400-450 °C and ~0.4-0.45 GPa are a realistic assumption (Fig. 6).

Sample KR4717 was collected in the central part of the Aar Massif (Central Alps, Switzerland), a late Variscan granitic intrusion. The location is a road cut ca. 3 km north of Andermatt. Qz, Pl, Kfs, Bt and Chl are the main constituents. Qz is recrystallized to ca. 100-300 µm large grains but mm-sized relics of magmatic Qz are present (Fig. 5b). During Alpine orogeny the sample experienced temperatures and pressures of up to ~420 °C and 0.28 GPa (Frey et al., 1980). A P-T path is not available for this part of the Alpine Lepontine metamorphism. However, based on a cooling P-T path of Qz in an extensional vein from the Aar Massif (Mullis, 1996), a P-T path for the studied sample can be inferred, which runs straight from maximum P-T to surface conditions (Fig. 6). The recrystallized grains are mostly free of internal deformation structures indicating static conditions during cooling and decompression.

Sample KR4874 comes from a quartzite layer in the contact aureole of the late Caledonian Ballachulish Igneous Complex (Scotland). It consists of up to 1 mm large, polygonal Qz grains with generally smaller Kfs grains and additional Kfs films along Qz grain boundaries (Fig. 5c). The lack of deformation features points to absence of deformation during and after contact metamorphism. Conditions of metamorphism and deformation of the contact aureole are discussed and summarized by Pattison and Voll (1991). The sample experienced a maximum of 655-670 °C and 0.3 GPa (Masch and Heuss-Aßbichler, 1991; Pattison, 1991) with subsequent isobaric cooling to ~250 °C. Maximum P-T conditions of regional metamorphism at the sample site are estimated ~450-550 °C and ~0.6 GPa (Fig. 6). For further details see Kruhl et al. (2013). In the past, this sample was analyzed by TEM, based on FIB sample preparation, resulting in 13 measurements of Qz grain boundaries (Kruhl et al., 2013). Here, we present 117 SEM measurements of opening widths of Qz grain boundaries and their correlation with grain size and crystallographic orientation of the boundaries.

Samples KR5184X and KR5185X were taken from pyrope (Prp) megablasts-bearing white schists in the Dora Maira Massif (Western Alps), at Case Tapina, Vallone di Gilba, and Case Ramello, south of Parigi, Valle di Po. At these localities, coesite (Coe) in rocks of the continental crust was first described (Chopin, 1984). In addition to Prp, the rocks consist mostly of phengite (Ph), Ky, talc (Tlc) and up to several hundred µm large Qz inverted from Coe (Fig. 5d). Starting with peak P-T conditions of more than 3.5 GPa and ~750-800 °C, the samples experienced nearly isothermal decompression, crossed the Coe-Qz transition at ~2.8 GPa and 750 °C and cooled to ~400 °C at ~0.5 GPa (Schertl et al., 1991). Then they followed a relatively straight P-T path to surface conditions (Fig. 6).

Samples KR2745A+B come from a pegmatite at Montescheno (Valle Antrona), ca. 3 km west of Villadossola (Val d'Ossola, Southern Alps, Italy), strongly deformed during Alpine (Lepontine) metamorphism at amphibolite facies conditions. Plagioclase completely recrystallized to ca. 150-200 µm large, mostly polygonal, slightly elongate grains (Fig. 5e) under dominantly static conditions indicating T of ~550 °C. This is based on correlations with grain sizes of recrystallized Pl in the south-western Lepontine heat dome (Altenberger et al., 1989) and in agreement with mineral zoning in the southwestern Lepontine Dome west of Val d'Ossola (Bousquet et al., 2004). The P-T development at the sample site is not well constrained. However, it can be inferred from the general P-T development in the southwestern Lepontine Dome (Borghi et al., 1996) that peak conditions of Lepontine metamorphism at ~550 °C and 0.35 GPa were followed by approximately constant cooling and decompression to surface conditions (Fig. 6).

Sample KR5329X1 is mm-sized peridotite from the western part of the Finero Ultramafic Complex, Variscan lower continental crust (Valle Cannobina, Southern Alps, Italy). In addition to Ol (forsterite), it contains Phl, Opx, Cpx, Amp and Chr (Fig. 5f). The rock experienced deformation under lowermost granulite facies conditions (Kruhl and Voll, 1976; Zingg, 1983); subsequent, late-Variscan cooling and decompression to lower greenschist facies conditions (Handy et al., 1999); and exhumation during the Alpine orogeny (Fig. 6).

4. Results

SEM imaging of grain boundaries in Qz aggregates at magnifications of up to 50,000 reveals characteristics of grain boundary networks as well as details at various locations along the boundaries. In most cases single grains are completely encapsulated by open boundaries, at least in 2D (Fig. 7a). Grain aggregates are traversed by networks of continuously open boundaries with µm-sized cavities along the boundaries or at triple junctions (Fig. 7b). The boundaries are several hundred nanometers wide with typically strictly parallel opposing grain faces (Figs. 7a, c and 8c) also clearly visible in TEM images (Figs. 1a, c and 3). They may be decorated with cavities, whereas subgrain boundaries are generally cavity-free (Figs. 7c, d and 8a). Often, cavities exhibit triangular shapes with one triangle apex away from the boundary, typical for dislocation-induced cavities (Billia et al., 2013; Kruhl et al., 2013).

Rarely, fracturing and opening of subgrain boundaries start at triple junctions with boundaries but typically fail after a short distance (Fig. 7d). Strong dissolution and precipitation lead to arrays of cavities encapsulating euhedral to subhedral crystal areas (Fig. 8a). Particularly large dissolution-precipitation cavities occur at triple junctions (Fig. 8b, c), with irregular or regular shapes and branches along the boundaries (Fig. 8b). Nearly all analyzed Qz and Pl grain boundaries are open (or filled with epoxy). Only in rare cases short sections of boundaries appear closed (Fig. 8b). In contrast, Ol boundaries in peridotite are filled with Srp, which does not replace Ol but fills the open space homogeneously and mostly with random orientation (Fig. 8d). A second stage of grain boundary fracturing and opening is indicated by open space between the Srp filling and the neighboring Ol. This space is generally smaller than the initial space between Ol grains (Fig. 9).

The widths of open Qz as well as Pl grain boundaries cover a range of up to ~500 nm, with median values of ~50 to ~200 nm, in one case around 200 nm (Fig. 9). Only the widths of the boundaries between up to several mm large Ol grains are in the range of several µm and Ol-Srp boundaries in the range of up to 1 µm. Most distributions are clearly left-asymmetric with median values smaller than the mean.

The c-axes of pairs of neighboring Qz grains were measured together with the crystallographic orientation of the boundary, that is, the grain boundary pole between them. The sum of the angles between the grain boundary pole and the two Qz c-axes provides a measure of the crystallographic orientation of the grain boundary in relation to both neighboring grains. A low total angle indicates a grain boundary pole close to the c-axes of both grains; a high total angle points to a grain boundary pole close to a-axes of both grains. No correlation exists between crystallographic orientation of grain boundaries and their widths for Qz in all analyzed four samples, exemplified for the two samples KR4874 and HH147B in Fig. 10.

Grain sizes of pairs of neighboring Qz grains were measured and the average area related to the width of the open boundary between the two grains. Again, nearly no correlation exists in all analyzed four samples, exemplified for sample KR4874 in Fig. 4. However, the relationship between grain area and width of open grain boundary shows a weak positive correlation amongst all analyzed samples (Fig. 11). This is true for the five Qz samples and specifically for samples KR5184X and KR5185X, which experienced the same retrograde P-T history after conversion of coesite to low-quartz (Fig. 6) but developed highly different grain sizes and grain boundary widths. Also Ol with its much larger grain sizes fits the correlation, whereas the widths of Pl grain boundaries show somewhat higher values than Qz grains of similar size. Even slightly higher grain sizes in 3D, due to the cut-effect, would not change this general relationship. The effect of temperature on grain-boundary width remains ambiguous. A sample with very high T-max (KR5185X) has similar Qz grain-boundary width than samples with low T-max (KR4717 and HH147B) or has clearly higher grain-boundary widths (KR5184X) or similar ones in comparison to a sample with lower T-max (KR4874).

The possible effect of the retrograde P-T path on the opening widths of the grain boundaries is examined (Fig. 12). The idea is that the present grain sizes together with the half volumes of the surrounding open boundaries (half, because of the contribution of both neighboring grains) represent the initial grain sizes at the P-T conditions of grain boundary fracturing and beginning widening. The difference between initial and present grain size, i.e. the percentage of volume change, depends on the elasticity data of the specific minerals. In the literature, the percentages of volume change are related to P-T conditions and can be plotted as contour lines in P-T diagrams. Consequently, fracturing and widening of grain boundaries start at P-T conditions, where these contour lines transect the P-T paths of the analyzed samples. P-T-related volume variation for Qz is given by Raz et al. (2002) and for Ol by Katsura et al. (2009). For Pl it can be estimated from the data of Steward and Limbach (1967) for temperature changes and Benusa et al. (2005) for pressure changes (Tab. 3). Based on these literature data, the contour lines of the 25th and 75th percentile of measurements of grain area and the median of grain-boundary opening width are determined for our samples. The determination scheme is given in table 2.

It should be kept in mind that, due to the cut-effect, the true 3D values of grain sizes are statistically slightly higher than the calculated ones. Accordingly, the true percentages of volume change are slightly lower than the calculated ones because the measured volume changes, that is, the true volumes of open boundaries are related to grain sizes which are statistically smaller than the true ones. For Qz, the volume percentage of open grain boundaries can be related to temperatures between ~300 °C and ~50 °C and pressures below ~0.35 GPa (Fig. 12a). For Ol, it can be related to temperatures between ~170 °C and ~85 °C and pressures below ~0.08 GPa (Fig. 12b). Pl shows slightly higher values: temperatures of ~330-210 °C at pressures of ~0.1-0.05 GPa (Fig. 12b, Tab. 3). However, the volume changes of Pl are given independently for T and P in the literature and the combined effect is accordingly slightly inaccurate. Other sources of inaccuracy must be considered: (i) the imprecision of the P-T paths of the different samples, even if it is limited for near surface conditions; (ii) especially for quartz the acute angles between the P-T paths and the contour lines of volume change, leading to larger T-shifts with small shifts of volume change.

5 Discussion

Grain boundaries of quartz, plagioclase and olivine and phase boundaries between olivine and serpentine from seven different samples have been measured by SEM and TEM. The grain boundaries of Qz and Pl are continuously open, mostly with constant width along the entire observable extension. Ol boundaries are nearly always filled with Srp. This means that also these boundaries were initially open. Even slightly open boundaries flatly inclined towards the section can be recognized as such under the applied high magnifications (Figs. 2 and 7a). In fact, directions of inclination can be determined and angles of inclination estimated and or precisely measured with the universal stage.

These observations show that most grains are completely separated in 2D (Figs. 2b and 7). Only few sections of boundaries are visible, which appear closed (Figs. 8b and 7c, d). Based on TEM measurements of 68 Qz grain boundaries, 33 published (Kruhl et al., 2013; Wirth et al., 2021) and 35 unpublished, the amount of open boundaries in Qz aggregates was estimated ~90 %, related to the total length of analyzed boundaries (Wirth et al., 2021). This value is confirmed by additional TEM measurements of grain and phase boundaries of Cal, Pl, Kfs, Crd, Sil, Srp, Amp, Opx, Cpx and Grt; 33 published (Wirth et al., 2021) and 18 unpublished. Closed sections can be clearly identified under HR-TEM. Based on a much larger data set, the present SEM investigations, too, confirm the value of ~90% total length of open grain boundaries, which should also hold for 3D. Such a high amount of open boundaries inevitably causes an extensive permeability. Consequently, the already observed connectivity of tubes along triple lines (White and White, 1981; Schenk and Urai, 2004) is complemented by a planar connectivity with accordingly increased permeability. Under which conditions this does occur will be discussed further below.

If ~90% of the grain and phase boundaries in rocks are open at the surface and in the uppermost part of the crust what holds the rocks together and ensures their strength? Firstly, after fracturing and widening the open boundaries are partially or totally filled with secondary minerals in the majority of rocks (Wirth et al., 2021). The boundaries between the fillings and the neighboring host grains are partially or totally closed. The fillings cause the cohesion of the rocks. Secondly, grain and phase boundaries are nearly always uneven. Their irregular geometry ranges from steps on the nanometer-scale to sutures of any shape and depth on the micrometer to millimeter-scale. They cause the strength of the rocks and guarantee that it is not possible to dismember a piece of rock easily even if grain and phase boundaries are totally open. Thirdly, the ~10% closed boundaries also contribute to the rock strength. However, currently the question about rock strength cannot be completely satisfactorily answered.

The extensive permeability allows access for larger amounts of fluids, if present. This may trigger dissolution-precipitation, specifically in Qz, already reported from various rocks (Watson and Brenan, 1987; Hippertt, 1994; Mancktelow et al., 1998; Mibe et al., 2003; Kruhl et al., 2013; Klevakina et al., 2014) and also leave imprints in the studied rock samples. Numerous mostly triangular cavities occur along open boundaries and at triple junctions (Figs. 1d; 7 and 8c, d) with crystallographically controlled faces (Fig. 8a). Such crystallographic control was also confirmed in previous studies (Mancktelow et al., 1998; Mancktelow and Pennacchioni, 2004; Billia et al., 2013; Kruhl et al., 2013; Wirth et al., 2021). The pyramidal shape and areal distribution of the cavities are a commonly presented feature in SEM investigations of broken surfaces of Qz crystal aggregates (Watson and Brenan, 1987; Mancktelow et al., 1998; Bestmann et al., 2011; Schmatz and Urai, 2011; Billia et al., 2013). These cavities were interpreted alternatively as (i) fluid inclusions along healed fractures (Hiraga et al., 1999), (ii) the result of grain boundary sliding (White, 1976; Behrmann, 1985; Mancktelow et al., 1998; Fusseis et al., 2009; Menegon et al., 2015), or (iii) accumulation of fluid during dynamic recrystallization (Mancktelow et al., 1998; Billia et al., 2013). Mancktelow and Pennacchioni (2004) notice that these cavities occur more frequently in 'wet' grain aggregates of a Qz-Fsp mylonite compared to 'dry' Qz aggregates. This is in agreement with our observation that grain boundaries in a late-Variscan Qz vein are strongly decorated with cavities of up to µm size (Fig. 7c, d) and show additional intensive dissolution features (Fig. 8a), although cavities are also present along grain boundaries in other samples. The interpretation of these cavities as dissolution pits generated by fluids in a permeable network of open grain and phase boundaries (Billia et al., 2013; Kruhl et al., 2013; Wirth et al., 2021) is backed by the observation that the cavities dominantly occur where dislocations or low angle boundaries meet open grain boundaries, i.e., at sites of increased solubility (Billa et al., 2013, Fig. 7a; Kruhl et al., 2013; Wirth et al., 2021, Fig. 9). In addition, variable occurrence of cavities may be caused by variable dissolubility at crystal faces of different crystallographic orientation (Benedová and Leichmann, 2016). Notably, dissolution pits are not present, or only in small numbers, along low-angle boundaries (Fig. 7c, d) and in aggregates of ultrafine Qz grains with almost entirely closed boundaries, where increased fluid flow cannot be expected (Bestmann et al., 2011, 2012). All this indicates that most dissolution cavities were generated during migration of fluids through open boundaries.

Ol grain boundaries are mostly filled with randomly oriented Srp (Fig. 8d), which neither grows at the expense of Ol nor as fibers perpendicular to the boundary typical of fiber veins (Ramsay and Huber, 1983; Passchier and Trouw, 2005, Chap. 6; Bons et al., 2012). It fills tubular dissolution cavities. Consequently, the boundaries were filled after initial opening. The Srp probably originates from a fluid infiltrating the open boundaries from larger depth.

The boundaries between Ol and Srp filling are mostly open (Fig. 8d). This indicates that the Ol grain aggregate did not cool, fracture, widen and fill with Srp under surface conditions but at elevated T, i.e., at a certain depth. This conclusion is supported by TEM observations of twofold opening of phase boundaries between sheet-silicate filling and surrounding grains of Qz, Amp and Px (Wirth et al., 2021 – Fig. 5, 8).

Kruhl et al. (2013) postulated that during exhumation Qz grain boundaries fracture and open due to cooling-related volume reduction below the transition from dominant crystal-plastic to brittle behavior of Qz, i.e., below ~300 °C (Voll, 1976; Stöckhert et al., 1999; Stipp et al., 2002), which is not balanced by decompression-related volume expansion. The strong P-T-related anisotropy of volume change (Ackermann and Sorrell, 1974; Levien et al., 1980; Kihara, 1990; Raz et al., 2002) leads to a larger width of grain boundaries perpendicular to Qz-<a> compared to grain boundaries perpendicular to Qz-[c]. The confining pressure telescopes the opening grain aggregate, so that boundaries perpendicular to Qz-[c] are preferentially closed while boundaries perpendicular to Qz-<a> remain partly open. At an amount of roughly 50% closed and 50% open boundaries the grain aggregate forms a stress-resistant framework that protects the still open boundaries of further closing (Kruhl et al., 2013). This model was initially backed by in total 19 TEM measurements of Qz grain boundary width and grain size, which show a weak correlation.

However, two observations indicate that the model cannot be true in detail. Firstly, as stated above, ~90% of the grain and phase boundaries are open in the range of up to several hundred nanometers. This is based on a much larger data set than the initial TEM investigation that led to the model. Secondly, grain boundaries perpendicular or at a high angle to Qz-<a> should be more widely open than boundaries at a high angle to Qz-[c]. However, a correlation between the crystallographic orientation of grain boundaries and their opening width does not exist in the analyzed Qz samples (Fig. 10). This does not necessarily argue against the concept that the anisotropic thermo-elasticity of Qz governs the opening of grain boundaries. A SEM study on a contact-metamorphic quartzite demonstrates that boundaries at high angles to Qz-<a> are statistically wider open than boundaries at high angles to Qz-[c] (Nagurney et al., 2021).

In general, the absence of a clear correlation in the analyzed quartz aggregates between the gap-width and the crystallographic orientation of the boundary may have different reasons. (i) Grain boundaries open at different times as suggested by 3D numerical modelling, combining contact mechanics and finite-element method (Raghami et al., 2020). This may lower the effect of anisotropic volume change. (ii) Grains may move relatively to each other during volume reduction under confining pressure. This may locally change grain boundary widths. Such movements have been observed under the TEM (Wirth et al., 2021 – Fig. 5A, 13) and are confirmed by 3D numerical modelling (Raghami et al., 2020). (iii) During volume reduction, the irregular shape of grains (Figs. 5 and 7) blocks their unimpeded movement and, therefore, reduces the effect of crystallography on the widening of grain boundaries. (iv) The variation of grain size, in combination with a low crystallographic preferred orientation of the quartz grains, may reduce the effect of the crystallographic orientation of the grain boundaries.

In each of the studied samples, the widths of open boundaries and the sizes of the bordering grains correlate only extremely weakly (Fig. 4). This at least partly results from the inaccurate size determination of grains of irregular shape and from the cut-effect that hampers inferring 3D sizes from 2D. In addition, as visible under the TEM as well as SEM, the grain aggregates may open along inter or intra-granular fractures (Figs. 2 and 5a,f), which may reduce the widening along neighboring grain boundaries. However, grain boundary widths and grain sizes correlate between the analyzed samples, which provide a much larger range of grain boundary width and grain size (Fig. 11). On a statistical basis, grain aggregates with larger grains have wider grain boundaries. This is true for Qz and specifically for the two samples KR5185X and KR5184X. They experienced the same maximum P-T conditions and the same retrograde P-T path but show clearly different grain boundary widths and grain sizes. Small grains are related to small grain boundary widths (KR5185X) and larger grains are related to larger grain boundary widths (KR5184X). The positive correlation between grain size and grain boundary width also holds if Qz, Pl and Ol are considered together. It is in agreement with the concept that the thermo-elastic properties of these minerals are mainly responsible for fracturing and widening of grain and phase boundaries.

Under which P-T-conditions do fracturing and widening take place? Principally, these processes can start as soon as cooling starts, i.e., at T between ~700 °C and ~400 °C for the analyzed minerals (Fig. 6). But such a scenario would require much larger grain boundary widths than measured, possible reduction by confining pressure not considered, and at least the occasional occurrence of higher-T fillings. However, up to now such fillings have not been observed, although low-T secondary minerals are widespread in grain and phase boundaries in a large variety of metamorphic and magmatic rocks (Wirth et al., 2021).

As a different approach, we compare the measured opening widths of the grain boundaries with the widths that would theoretically develop from fracturing and widening of the boundaries during cooling and decompression up to surface conditions (Tab. 2 and 3, Fig. 12). Such comparison results in P-T conditions of fracturing of grain boundaries with subsequent widening at ~300 to ~50 °C and up to ~0.35 GPa for Qz (Fig. 12a) and ~170 to ~85 °C and ~0.08 GPa for Ol (Fig. 12b).

Estimations for Pl suggest ~330 to ~210 °C and ~0.1-0.05 GPa (Fig. 12b). How realistic are these values? Given that grain sizes inferred from grain areas are generally slightly lower than the true ones, the estimated P-T values appear potentially even too high. In addition, inaccuracies are introduced by inaccurate determinations of grain areas, grain boundary widths and P-T paths. The small angles between the contour lines of cooling-decompression related volume change and the P-T paths, specifically for Qz, may lead to further inaccuracy. Independently, the estimated T and P may be too low if open boundaries were partly closed by the confining pressure during exhumation. However, this is contradicted by the observation that at least 90% of the grain boundaries are open and that only low-T minerals have been found so far as fillings of open grain boundaries (sheet silicate, chlorite, serpentine) and only in rare cases minerals that may form at lowermost greenschist facies conditions (biotite, actinolite) (Wirth et al., 2021). It is additionally contradicted by the observation that fibrous fillings of grain and phase boundaries are nearly never even slightly deformed (Fig. 8d; Wirth et al., 2021 – Fig. 6, 8, 12). On the other hand, opening under ambient conditions can be largely excluded due to (i) the occurrence of minerals like biotite and actinolite, and (ii) the observation that also phase boundaries between secondary, low-T minerals and the adjoining host grains fracture and widen. This indicates ongoing volume reduction after filling of open boundaries.

Furthermore, 3D grain-scale numerical modelling of grain boundary fracturing and widening in Qz grain aggregates shows that fracturing of Qz grain boundaries starts at ~220 °C, assuming that the thermo-elastic strain becomes operative below the transition from dominant crystal-plastic to brittle behavior of Qz, i.e., below ~300 °C (Raghami et al., 2020). This T-difference is related to the tensile yield strength of the boundaries, which has to be overcome. In this context, it is worth mentioning that Qz grain aggregates with grain sizes of only a few µm or below do not show considerable widening, if at all (Fitz Gerald et al., 2006; Bestmann et al., 2012).

In summary, independently of various uncertainties of measurements and T-estimations and based on observations and data sets available in the literature, it becomes clear that fracturing and widening of grain boundaries in the investigated grain aggregates of quartz, plagioclase and olivine take place under low T and P conditions. Such conditions are well below the transitions from crystal-plastic to brittle behavior of these minerals. Consequently, the experienced peak conditions of metamorphism or magma crystallization do not affect the fracturing and the widths of open or refilled grain boundaries.

6. Conclusions

Our investigation shows that a modern SEM is able to measure open grain and phase boundaries with sufficient precision and at the same time this method allows to obtain a data volume that is large enough for statistically sound conclusions. However, large magnifications are necessary, preferably more than five to ten thousand times. SEM bridges the gap between high-precision TEM measurements on small sample volumes and the relatively inaccurate measurements on large sample volumes with the polarized-light microscope. The combination of these methods allows the investigation of grain and phase boundaries and their networks from the nanometer to the millimeter scale, i.e., over about 6-7 orders of magnitude.

Totally or partially open grain and phase boundaries at higher crustal levels and at the surface cause permeability, provide the opportunity for extensive fluid flow and, consequently, affect physical properties of rocks and a variety of geological processes. In addition, it should be tested if open boundaries also occur in other crystalline materials, such as ceramics or metals, with similar effects on material properties and processes.

The results of our investigations neither indicate nor disprove the occurrence of networks of totally or partially open grain and phase boundaries under higher P-T conditions, e.g., at mid-crustal levels. Quartz boundaries are most probably not open at such depth but grain boundaries of other minerals, such as feldspars, pyroxenes or amphiboles, with a much higher transition temperature from crystal-plastic to brittle behavior may be open. The investigations to date are still too limited for such statements and studies on a larger variety of rocks with different mineralogy and different P-T histories are necessary. Furthermore, data sets measured by a wide variety of methods need to be acquired and compared.

Acknowledgements

We gratefully acknowledge the help of Anja Schreiber, who prepared the TEM foils with FIB. Thanks are due to Günter Buntebarth for providing a sample from the Ballachulish contact aureole, to Peter Gille for providing access to and help with a high-precision saw, to Guntram Jordan for a useful discussion, and to John Platt, an anonymous reviewer and Virginia Toy for detailed and helpful reviews. The investigations were financially supported by the German Research Council (DFG) under grant SCHM390/17-1 / KR691/36-1.

References

Altenberger, U., Hamm, N., Kruhl, J.H., 1987. Movements and metamorphism north of the Insubric Line between Val Loana and Val d'Ossola, N.Italy. Jahrbuch Geologische Bundesanstalt Wien 130(4), 365-374.

Ackermann, R.J. and Sorrell, C.A., 1974. Thermal expansion and the high-low transformation in Quartz. I. High-temperature X-ray studies. Journal of Applied Crystallography 7, 461-467.

Aust, K.T., Erb, U., Palumbo, G., 1994. Interface control for resistance to intergranular cracking. Materials Science and Engineering A 176, 329-334.

Behrmann, J.H., 1985. Crystal plasticity and superplasticity in quartzite: a natural example. Tectonophysics 115, 101-129.

Bell, I.A. and Wilson, C.J.L., 1981. Deformation of biotite and muscovite: TEM microstructure and deformation model. Tectonophysics 78, 201-228.

Benedová, Š. and Leichmann, J., 2016. Experimental study of anisotropy of quartz dissolution and its role in fluid migration in rocks. Acta Geodynamica et Geomaterialia 13(2), 193–200, https://doi.org/10.13168/AGG.2016.0001.

Benusa, M.D., Angel, R.J., Ross, N.L. (2005). Compression of albite, $NaAlSi_3O_8$. American Mineralogist 90, 1115-1120, https://doi.org/10.2138/am.2005.1805.

Bestmann, M., Pennacchioni, G., Frank, G., Göken, M., de Wall, H., 2011. Pseudotachylyte in muscovite-bearing quartzite: Coseismic friction-induced melting and plastic deformation of quartz. Journal of Structural Geology 33, 169-186, https://doi.org/10.1016/j.jsg.2010.10.009.

Bestmann, M., Pennacchioni, G., Nielsen, S., Göken, M., de Wall, H., 2012. Deformation and ultrafine dynamic recrystallization of quartz in pseudotachylyte-bearing brittle faults: A matter of a few seconds. Journal of Structural Geology 38, 21-38, https://doi.org/10.1016/j.jsg.2011.10.001.

Billia, M.A., Timms, N.E., Toy, V.G., Hart, R.D., Prior, D.J., 2013. Grain boundary dissolution porosity in quartzofeldspathic ultramylonites: Implications for permeability enhancement and weakening of mid-crustal shear zones. Journal of Structural Geology 53, 2-14, http://dx.doi.org/10.1016/j.jsg.2013.05.004.

Borghi, A., Compagnoni, R., Sandrone, C., 1996. Composite P-T paths in the Internal Penninic Massifs of the Western Alps: Petrological constraints to their thermo-mechanical evolution. Eclogae geologicae Helvetiae 89(1), 345-367.

Bohlen, S.R., Montana, A., Kerrick, D.M., 1991. Precise determinations of the equilibria kyanite - sillimanite and kyanite - andalusite and a revised triple point for Al_2SiO_5 polymorphs. American Mineralogist 76(3-4), 677-680.

Bons, P.D., Elburg, M.A. Gomez-Rivas, E., 2012. A review of the formation of tectonic veins and their microstructures. Journal of Structural Geology 43, 33-62, http://dx.doi.org/10.1016/j.jsg.2012.07.005.

Bousquet, R., Engi, M., Gosso, G., Oberhänsli, R., Berger, A., Spalla, M.I., Zucali, M., Goffè, B., 2004. Explanatory notes to the map: metamorphic structures of the Alps – transition from the Western to the Central Alps. Mitteilungen der Österreichischen Mineralogischen Gesellschaft 149, 145-156.

Bukovská, Z., Wirth, R., Morales, L.F., 2015. Pressure solution in rocks: focused ion beam / transmission electron microscopy study on orthogneiss from South Armorican Shear Zone, France. Contributions to Mineralogy and Petrology 170:31, https://doi.org/10.1007/s00410-015-1186-8.

Burnard, P.G., Demouchy, S., Delon, R., Arnaud, N.O., Marrocchi, Y., Cordier, P., Addad, A., 2015. The role of grain boundaries in the storage and transport of noble gases in the mantle. Earth and Planetary Science Letters 430, 260–270, http://doi.org/10.1016/j.epsl.2015.08.024.

Chopin, C., 1984. Coesite and pure pyrope in high-grade blueschists of the Western Alps: a first record and some consequences. Contributions to Mineralogy and Petrology 86, 107-118.

Delvigne, J. E., 1998. Atlas of micromorphology of mineral alteration and weathering. The Canadian Mineralogist, Special Publication 3. Mineralogical Association of Canada, 494 pp.

Doukhan, J.-C., Trepied, L., 1979. Plasticity of quartz: crystallographic models and T.E.M. Observations. Bulletin de minéralogie 102, 138-147.

Duyster, J., Stöckhert, B., 2001. Grain boundary energies in olivine derived from natural microstructures. Contributions to Mineralogy and Petrology 140, 567-576, https://doi.org/10.1007/s004100000200.

Fitz Gerald, J.D., Mancktelow, N.S., Pennacchioni, G., Kunze, K., 2006. Ultrafine-grained quartz mylonites from high-grade shear zones: Evidence for strong dry middle to lower crust. Geology 34(5), 369–372, https://doi.org/10.1130/G22099.1.

Frary, M., Schuh, C.A., 2005. Grain boundary networks: scaling laws, preferred cluster structure, and their implications for grain boundary engineering. Acta Materialia 53, 4323-4335.

Freitag, S., Klaver, J., Malai, I.S., Klitzsch, N., Urai, J.L., Stollhofen, H., Bauer, W., Schmatz, J., 2022. Petrophysical characterization, BIB-SEM imaging, and permeability models of tight carbonates from the Upper Jurassic (Malm ß), SE Germany. Geothermal Energy 10:30, https://doi.org/10.1186/s40517-022-00239-x

Frey, M., Bucher, K., Frank, E., 1980. Alpine metamorphism along the geotraverse Basel-Chiasso: a review. Eclogae Geologicae Helvetiae 73(2), 527-546.

Frey, M., Ferreiro Mählmann, R. (1999). Alpine metamorphism of the Central Alps. Schweizerische mineralogische und petrographische Mitteilungen 79, 135-154.

Fusseis, F., Regenauer-Lieb, K., Liu, J., Hough, R.M., De Carlo, F., 2009. Creep cavitation can establish a dynamic granular fluid pump in ductile shear zones. Nature Letters 459, https://doi.org/10.1038/nature08051.

Gross, A.F.K., Van Heege, J.P.T., 1973. The high-low quartz transition up to 10 kb pressure. Journal of Geology 81, 717-724.

Handy, M.R., Franz, L., Heller, F., Janott, B., Zurbrigg, R., 1999. Multistage accretion and exhumation of the continental crust (Ivrea crustal section, Italy and Switzerland). Tectonics 18(6), 1154-1177.

Helbing, H., 2003. No suture in the Sardinian Variscides: a structural, petrological, and geochronological analysis. Tübinger Geowissenschaftliche Arbeiten, Reihe A 68, 1–190, http://w210.ub.uni-tuebingen.de/dbt/

Hippertt, J.F., 1994. Microstructures and c-axis fabrics indicative of quartz dissolution in sheared quartzites and phyllonites. Tectonophysics 229, 141-163.

Hiraga, T., Nagase, T., Akizuki, M., 1999. The structure of grain boundaries in granite origin ultramylonite studied by high-resolution electron microscopy. Physics and Chemistry of Minerals 26(8), 617–623, https://doi.org/10.1007/s002690050.

Hovis, G.L., Medford, E., Conclon, M., Tether, A., Romanovski, A., 2010. Principles of thermal expansion in the feldspar system. American Mineralogist 95, 1060–1068, https://doi.org/10.2138/am.2010.3484

Huang, W.L., Wyllie, P.J., 1981. Phase relationship of S-type granite with H_2O to 35 Kbar: muscovite granite from Harney Peak, South Dakota. Journal of Geophysical Research 86(B11), 1015–1029.

Katsura, T., Shatskiy, A., Geeth, M.A., Manthilake, M, Zhai, S., Fukuia, H., Yamazaki, D., Matsuzaki, T., Yoneda, A., Ito, E., Kuwata, A., Ueda, A., Nozawa, A., Funakoshi, K.-I., 2009. Thermal expansion of forsterite at high pressures determined by in situ X-ray diffraction: The adiabatic geotherm in the upper mantle. Physics of the Earth and Planetary Interiors 174, 86–92, https://doi.org/10.1016/j.pepi.2008.08.002.

Kerrick, D.M., 1968. Experiments on the upper stability limit of pyrophyllite at 1.8 kilobars and 3.9 kilobars water pressure. American Journal of Science 266(3), 204-214. https://doi.org/10.2475/ajs.266.3.204

Kihara, K., 1990. An X-ray study of the temperature dependence of the quartz structure. European Journal of Mineralogy 2(1), 63-77.

Klevakina, K., Renner, J., Doltsinis, N., Adeagbo, W., 2014. Transport processes at quartz–water interfaces: constraints from hydrothermal grooving experiments. Solid Earth 5, 883–899, https://doi.org/10.5194/se-5-883-2014

Kruhl, J.H., 1993. The P-T-d development at the basement-cover boundary in the north-eastern Tauern Window (Eastern Alps): Alpine continental collision. Journal of metamorphic Geology 11(1), 31-47.

Kruhl, J.H., Voll, G., 1976. Fabrics and Metamorphism from the Monte Rosa Root Zone into the Ivrea Zone near Finero, Southern Margin of the Alps. Schweizerische mineralogische und petrographische Mitteilungen 56, 627-633.

Kruhl, J.H., Wirth, R., Morales, L.F.G., 2013. Quartz grain boundaries as fluid pathways in metamorphic rocks. Journal of Geophysical Research Solid Earth 118(5), 1-11. https://doi.org/10.1002/jgrb.50099.

Levien, L., Prewitt, C.T., Weidner, D.J., 1980. Structure and elastic properties of quartz at pressure. American Mineralogist 65(9-10), 920-930.

Mainprice, D., Lloyd, G.E., Casey, M. (1993). Individual orientation measurements in quartz polycrystals – advantages and limitations for texture and petrophysical property determinations. Journal of Structural Geology 15, 1169-1187.

Mancktelow, N.S, Grujic, D., Johnson, E.L. (1998). An SEM study of porosity and grain boundary microstructure in quartz mylonites, Simplon Fault Zone, Central Alps. Contributions to Mineralogy and Petrology 131(1), 71-85.

Mancktelow, N.S., Pennacchioni, G., 2004. The influence of grain boundary fluids on the microstructure of quartz-feldspar mylonites. Journal of Structural Geology 26(1), 47-69.

Masch, L., Heuss-Aßbichler, S., 1991. Decarbonation reaction mechanisms of carbonate rocks: a comparison between the thermoaureoles of Ballachulish and Monzoni (N. Italy). In: Voll, G. et al. (Eds), Equilibrium and Kinetics in Contact Metamorphism. The Ballachulish Igneous Complex and Its Aureole, Springer, Berlin/Heidelberg/New York, 229–249.

Menegon, L., Fusseis, F., Stünitz, H., Xiao, X., 2015. Creep cavitation bands control porosity and fluid flow in lower crustal shear zones. Geology 43(3), 227–230, https://doi.org/10.1130/G36307.1.

Mibe, K., Yoshino, T., Ono, S., Yasuda, A., Fujii, T., 2003. Connectivity of aqueous fluid in eclogite and its implications for fluid migration in the Earth's interior. Journal of Geophysical Research 108(B6), 2295, https://doi.org/10.1029/2002JB001960.

Mullis, J., 1996. P-T-t path of quartz formation in extensional veins of the Central Alps. Schweizerische mineralogische und petrographische Mitteilungen 76(2), 159-164.

Nagurney, A.B., Caddick, M.J., Law, R.D., Ross, N.L., Kruckenberg, S.C., 2021. Crystallographically controlled void space at grain boundaries in the Harkless quartzite. Journal of Structural Geology 143, https://doi.org/10.1016/j.jsg.2020.104235.

Nicolas, A., Poirier, J.-P., 1976. Crystalline Plasticity and Solid State Flow in Metamorphic Rocks. Wiley, New York.

Passchier, C.W., Trouw, R.A.J., 2005. Microtectonics. 2nd edition, Springer, Berlin/Heidelberg/New York.

Pattison, D.R.M., 1991. P-T-a(H2O) conditions in the thermal aureole. In: Voll, G. et al. (Eds.), Equilibrium and Kinetics in Contact Metamorphism. The Ballachulish Igneous Complex and Its Aureole. Springer, Berlin/Heidelberg/New York, 327–350.

Pattison, D.R.M., Voll, G., 1991. Regional geology of the Ballachulish area. In: Voll, G. et al. (Eds.), Equilibrium and Kinetics in Contact Metamorphism. The Ballachulish Igneous Complex and Its Aureole. Springer, Berlin/Heidelberg/New York, 19–36.

Price, J.D., Wark, D.A., Watson, E.B., Smith, A.M., 2006. Grain-scale permeabilities of faceted polycrystalline aggregates. Geofluids 6(4), 302–318, doi:10.1111/j.1468-8123.2006.00149.x.

Raghami, E., Schrank, C., Kruhl, J.H., 2020. 3D modelling of the effect of thermal-elastic stress on grain-boundary opening in quartz grain aggregates. Tectonophysics 774, 1-13, https://doi.org/10.1016/j.tecto.2019.228242.

Ramsay, J.G., Huber, M.I., 1983. The Techniques of Modern Structural Geology. Vol. 1: Strain Analysis. Academic Press, Inc., London.

Raz, U., Girsperger, S., Thompson, A.B., 2002. Thermal expansion, compressibility and volumetric changes of quartz obtained by single crystal dilatometry to 700°C and 3.5 kilobars (0.35 GPa). Schweizerische mineralogische und petrographische Mitteilungen 82(3), 561–574, http://doi.org/10.5169/seals-62381.

Schenk, O., Urai, J.L., 2004. Microstructural evolution and grain boundary structure during static recrystallization in synthetic polycrystals of Sodium Chloride containing saturated brine. Contributions to Mineralogy and Petrology 146(6), 671–682, doi:10.1007/s00410-003-0522-6.

Schenk, O., Urai, J.L., Piazolo, S., 2006. Structure of grain boundaries in wet, synthetic polycrystalline, statically recrystallizing halite – evidence from cryo-SEM observations. Geofluids 6, 93–104.

Schertl, H.-P., Schreyer, W., Chopin, C., 1991. The pyrope-coesite rocks and their country rocks at Parigi, Dora Maira Massif, Western Alps: detailed petrography, mineral chemistry and PT-path. Contributions to Mineralogy and Petrology 108, 1–21.

Schmatz, J., Urai, J.L., 2011. The interaction of migrating grain boundaries and fluid inclusions in naturally deformed quartz: A case study of a folded and partly recrystallized quartz vein from the Hunsrück Slate, Germany. Journal of Structural Geology 33, 468-480, https://doi.org/10.1016/j.jsg.2010.12.010.

Shimada, M., Kokawa, H., Wang, Z.J., Sato, Y.S., Karibe, I., 2002: Optimization of grain boundary character distribution for intergranular corrosion resistant 304 stainless steel by twin-induced grain boundary engineering. Acta Materialia 50, 2331-2341.

Stewart, D.B., von Limbach, D., 1967. Thermal expansion of low and high albite. The American Mineralogist 52, 389-413.

Stipp, M., Stünitz, H., Heilbronner, R., Schmid, S.M., 2002. The eastern Tonale fault zone: A ‘natural laboratory’ for crystal plastic deformation of quartz over a temperature range from 250 to 700 °C. Journal of Structural Geology 24(12), 1861–1884, https://doi.org/10.1016/S0191-8141(02)00035-4.

Stöckhert, B., Brix, M.R., Kleinschrodt, R., Hurford, A.J., Wirth, R., 1999. Thermochronometry and microstructures of quartz – a comparison with experimental flow laws and predictions on the temperature of the brittle-plastic transition. Journal of Structural Geology 21, 351-369.

Tullis, J., 1983. Deformation of feldspars. Reviews in Mineralogy 2, 297-323.

Vernon, R.H., 2004. A practical guide to rock microstructure. Cambridge University Press, 594 pp.

Voll, G., 1960. New work on petrofabrics. Liverpool and Manchester Geological Journal 2, 503-567.

Voll, G., 1976. Recrystallization of quartz, biotite and feldspars from Erstfeld to the Leventina Nappe, Swiss Alps, and its geological significance. Schweizerische mineralogische und petrographische Mitteilungen 56, 641-647.

Watson, E.B., Brenan, J.M., 1987. Fluids in the lithosphere, 1. Experimentally-determined wetting characteristics of CO_2-H_2O fluids and their implications for fluid transport, host-rock physical properties, and fluid inclusion formation. Earth and Planetary Science Letters 85, 497-515.

White, S., 1976. The role of dislocation processes during tectonic deformations, with particular reference to quartz. In: Strens, R.J. (Ed.), The Physics and Chemistry of Minerals. Wiley-Interscience, London, 75-91.

White, J.C., White, S.H., 1981. On the structure of grain boundaries in tectonites. Tectonophysics 78, 613-628.

Whitney, D., Evans, D.W., 2010. Abbreviations for names of rock-forming minerals. American Mineralogist 95, 185–187, https://doi.org/10.2138/am.2010.3371.

Wirth, R., 2009. Focused Ion Beam (FIB) combined with SEM and TEM: Advanced analytical tools for studies of chemical composition, microstructure and crystal structure in geomaterials on a nanometre scale. Chemical Geology 261, 217–229, https://doi.org/10.1016/j.chemgeo.2008.05.019.

Wirth, R., Kruhl, J.H., Morales, L.F.G., Schreiber, A., 2021. Partially open grain and phase boundaries as fluid pathways in magmatic and metamorphic rocks. Journal of Metamorphic Geology 40, 65-87, https://doi.org/10.1111/jmg.12610.

Yardley, B.W.D., 1989. An introduction to metamorphic petrology. Longman Group, 248 pp.

Zingg, A., 1983. The Ivrea and Strona-Ceneri Zones (Southern Alps, Ticino and N-Italy) – A Review. Schweizerische mineralogische und petrographische Mitteilungen 63, 361-392.

Captions

Figure 1

TEM and SEM images of Qz grain boundaries. **(a)** HAADF TEM image of an open Qz grain boundary from a jadeite quartzite (Shuanghe, Dabie–Sulu Belt, Central Eastern China). The light band (Pt) is a protective layer of platinum covering the thin-section surface prior to FIB milling. A small depression occurs where the grain boundary meets the thin-section surface. Sample RP11, foil 3344. **(b)** SEM image of a Qz grain boundary. Irregular depressions on both sides along the boundary were generated by grinding and polishing of the thin section. The open boundary with sharp parallel crystal faces on both sides is clearly visible (arrow). Locally, relics of epoxy cover the boundary margins (double arrows). Quartzite from the contact aureole of the late Caledonian Ballachulish Igneous Complex (Scotland). Sample KR4874. **(c)** HAADF TEM image of an open Qz grain boundary from the same sample. Modified figure 2b from Kruhl et al. (2013). The light band (Pt) is a protective layer of platinum covering the thin-section surface prior to FIB milling. A small grain fragment (white arrow) is rotated into the open grain boundary (curved black arrow), probably during thin-section polishing. Platinum fills the open space at the tip of the grain boundary (double arrow). Sample KR4874, foil 2075. **(d)** SEM image of three open Qz grain boundaries (black arrows) and their triple junction. Along the boundaries the grains are partly fragmented (x) and excavated, due to grinding during thin-section preparation. Excavation is particularly large at the triple junction, where the boundaries form a triangular cavity (white arrow). Sample HH147B-3; Qz vein in the late Variscan basement of the Baronie (eastern Sardinia, Italy).

Figure 2

Polarized-light photomicrograph with crossed polarizers and gypsum test plate **(a)** and SEM (BSE mode) image **(b)** of a network of continuously open grain boundaries in an aggregate of polygonal Pl grains. Sample KR2745A-1, section perpendicular to foliation and lineation. Inspections at magnifications of up to 30k show that the boundaries are open even if appearing closed at lower magnifications in the polarized-light image or the SEM image (short open arrows). They may be widened by fractures that locally transect grains (long arrows). Flatly dipping open boundaries lead to excavations at the thin-section surface (asterisks). Tiny spots are mostly due to grinding and polishing.

Figure 3

TEM images of open, kinked Qz grain boundaries. **(a)** HAADF TEM image of a Qz grain boundary in Cambrian quartzite („Pipe Rock“) from the Moine Thrust Zone at Loch Assynt (Scotland). Sample KR4970-1; foil 6104. The kinks of the open boundary between the perfectly matching faces of the opposite grains Qz1 and Qz2 indicate displacement of the grains by ~60 nm parallel to the horizontal white lines. The longer sections of the boundary in the lower left and upper right parts of the image are only ~30 nm wide (thick, short white line). Numerous subgrain boundaries are interspersed throughout the grains (white arrows). Where they meet the open boundary, cone-shaped euhedral dissolution cavities occur (double arrow). Euhedral black spots represent fluid inclusions. **(b)** TEM bright-field image of a Qz grain boundary in hydrothermal Qz from the 'Pfahl' (Bavarian Forest, Germany). Sample KR5095A-3; foil 5840. The kinks of the open boundary between the perfectly matching faces of the opposite grains Qz1 and Qz2 indicate displacement of the grains by ~260 nm parallel to the black lines. The widths of the different boundary sections of ~230 nm and 145 nm (black double lines) are clearly lower. The white double arrow points to a cone-shaped dissolution cavity where a dislocation meets the open boundary.

Figure 4

Relationship between grain area and width of open Qz grain boundary, based on SEM and TEM measurements. The latter are taken from Kruhl et al. (2013) and recalculated for grain area instead of grain diameter. For the one measurement outside the diagram the grain area is given. Broken lines mark the 25th and 75th percentiles for grain area and boundary width. Sample KR4874; quartzite from the contact aureole of the late Caledonian Ballachulish Igneous Complex (Scotland).

Figure 5

Photomicrographs of the studied samples; all with crossed polarizers and gypsum plate inserted for better distinction between the different grains. **(a)** Sample HH147B-5: Qz vein from the late Variscan basement of the Baronie (eastern Sardinia, Italy). Long grain axes represent the main regional foliation. Strongly lobate grain boundaries result from deformation under greenschist facies conditions and, locally, form a second generation of small recrystallized grains (arrows). A network of partly open cracks transects the material (double arrows). **(b)** Sample KR4717: late Variscan granite (Aar Massif, Central Alps, Switzerland) deformed and recrystallized under lower greenschist facies conditions. Relics of magmatic Qz with subgrain boundaries are preserved (X). Magmatic Pl shows strong alteration (saussuritization) due to prograde Alpine ('Lepontine') metamorphism. **(c)** Sample KR4874: quartzite from the contact aureole of the late Caledonian Ballachulish Igneous Complex (Scotland) with up to 1 mm large, roughly polygonal Qz and typically smaller Kfs. Recrystallized Qz from regional greenschist facies deformation and metamorphism coarsened during contact metamorphism. Kfs forms thin layers along Qz grain boundaries (arrows). **(d)** Sample KR5185X: polygonal Qz grain aggregate in a white schist from the Dora Maira Massif at (Case Ramello/Parigi, Valle di Po, and Case Tapina, Vallone di Gilba, Western Alps). In addition to Prp-megablasts and Qz, white mica (Ph) and Ky are frequent. The photomicrograph is also representative of sample KR5184X. **(e)** Sample KR2745B-3x: pegmatite from the southwestern Lepontine heat dome (Western Alps) deformed under lower amphibolite-facies conditions; aggregate of roughly polygonal, weakly elongate, recrystallized Pl grains (albite); section parallel to the main regional foliation. The long grain axes represent the lineation parallel to the short side of the image. **(f)** Sample KR5329X1: phlogopite peridotite from the Finero Ultramafic Complex, Variscan lower continental crust, Southern Alps (Valle Cannobina, Northern Italy). In addition to Ol (forsterite) and Phl, the rock contains partly euhedral Chr (black) and Cpx.

Figure 6

P-T paths of the investigated samples. Stability fields of Al_2SiO_5 polymorphs after Bohlen et al. (1991); upper stability limit of pyrophyllite (Pyp) after Kerrick (1968); wet granite solidus (wgs) after Huang and Wyllie (1981); low–high quartz transition (L/H) after Gross and Van Heege (1971);

approximate temperature threshold for dislocation creep ('brittle-ductile transition'; Nicolas and Poirier, 1976) of various minerals, equivalent to recrystallization temperatures, with an uncertainty of ±10–15°C: Qz (Voll, 1976; Stöckhert et al., 1999; Stipp et al., 2002), Fsp (Pl and Kfs) (Voll, 1976; Tullis, 1983; Altenberger et al., 1987; Kruhl, 1993). (1) Sample HH147B, Baronie (Eastern Sardinia, Italy); (2) sample KR4717, Aar Massif (Central Alps, Switzerland); (3) sample KR4874, contact aureole of the Ballachulish Igneous Complex (Scotland); (4) samples KR5184X and KR5185X, Dora Maira Massif (Vallone di Gilba and Valle di Po, Western Alps, Italy); (5) samples KR2745A and B, Valle Antrona, Western Alps (Italy); (6) sample KR5329X1, Valle Cannobina (Western Alps, Italy).

Figure 7

SEM images of open Qz grain boundaries. **(a)** 20-30 µm sized grain completely encapsulated by up to 100 nm wide open boundaries. Excavated domains along the boundaries (arrows) are due to thin-section preparation. Cavities at a triple junction (double arrow) arise from dissolution-precipitation. BSE image; sample HH147B-8; Qz vein from the Orune Schists, Baronie (Sardinia, Italy). **(b)** Network of completely open boundaries in an aggregate of polygonal grains of recrystallized Qz. White arrows point to dissolution-precipitation related cavities along the boundaries and at triple junctions. SE image; sample KR4717; meta-granite, Aar Massif (Central Alps, Switzerland). **(c)** Continuously open Qz boundaries, locally with healed boundaries with cavities (short, thick, open arrow). The open boundaries are decorated with 1-2 µm large cavities (short arrows), whereas the numerous subgrain boundaries are generally cavity-free. The grains contain µm-sized probably primary inclusions. Healing of cracks led to arrays of inclusions (double arrows). BSE image; sample HH147B-5; Qz vein from the Orune Schists, Baronie (Sardinia, Italy). **(d)** Continuously open boundaries between polygonal Qz grains, locally with dissolution-precipitation cavities (short arrows). The subgrain boundaries (asterisk) are almost completely cavity-free. Incomplete opening from triple junctions along subgrain boundaries rarely occurs (double arrows). BSE image; sample HH147B-3; Qz vein from the Orune Schists, Baronie (Sardinia, Italy).

Figure 8

SEM images of open Qz and Ol grain boundaries. **(a)** Qz boundary with numerous, several µm-large cavities. Euhedral to subhedral crystal fragments (x) are shaped by dissolution and precipitation. Subgrain boundaries (arrows) are nearly free of cavities. BSE image; sample HH147B3; Qz vein from the Orune Schists, Baronie (Sardinia, Italy). **(b)** Several µm-sized dissolution-precipitation cavities at a triple junction (x) and along Qz grain boundaries (arrows). A section of the boundary appears closed on the thin-section surface (double arrow). SE image; sample KR4874-3; quartzite from the contact of the Ballachulish Complex (Scotland). **(c)** Junction of three 200-250 nm thick, open Qz grain boundaries. Opposing grain faces are mostly parallel except dissolved parts of grains marked by broken lines. Grain boundary kinks indicate directions of opening (double arrows). The boundaries are mostly filled with epoxy (whitish, grainy material). SE image; sample KR4874-2. **(d)** Approx. 4 µm thick boundary between two Ol grains, filled with serpentine (Srp), determined by TEM EDX. Srp is randomly oriented as shown by its spotty appearance. Short, thick arrow indicates tubular dissolution cavity filled with Srp. Several hundred nm-wide stripes of open space (black) occur between Srp and both neighboring Ol grains. Conical dissolution-precipitation cavities generated prior to Srp-filling indicate opening oblique to the Srp-Ol boundary (white arrows). Asterisks mark excavations due to sample preparation. BSE image; sample KR5329X1-4; peridotite (Finero Complex, Southern Alps, Italy).

Figure 9

Frequency distribution of grain boundary widths for Qz (a-d), Pl (e-f), Ol-Srp (g), and Ol (h). Sample numbers and numbers of measurements n are given. For sample KR5184X, one measurement of grain boundary width is outside the presented interval. The three arrows below each diagram indicate (from left to right) 25^{th} percentile, median, and 75^{th} percentile.

Figure 10

Relationship between (i) the angles of c-axes of pairs of Qz grains and the pole of the grain boundary between them and (ii) the width of the (open) grain boundary, exemplified by the samples KR4874 (left) and HH147B (right). The two angles α_1 and α_2 between the pole P of the grain boundary (double line) and the two Qz-c axes c_1 and c_2, as shown in the sketch, are added. They range between 0 and 180°. A low total angle indicates a grain boundary pole close to the c-axes of both grains; a high total angle points to a grain boundary pole close to the a-axes of both grains. Qz-c orientations and grain boundary poles were measured by universal stage.

Figure 11

Double-logarithmic plot of grain area versus width d of open grain boundary, based on SEM measurements of Qz as well as Pl, Ol and Srp from eight different samples with various P-T-deformation histories presented in figure 6. For each sample the 25th and 75th percentiles of grain boundary width d and grain area are presented (boxes) as well as median (circle), mean (+), the number of measurements n and the maximum temperature experienced by the sample. The samples KR2745A-1 and KR2745B-3x are from the same deformed pegmatite with flat, elongate, recrystallized Pl grains. The analyzed section of the first sample is cut perpendicular to the lineation and foliation (YZ section) (Fig. 2) and the section of the second sample parallel to the foliation (XY section) (Fig. 5e). Based on the measured areas and the X, Y, Z ratios taken from photomicrographs, the grain volumes are calculated and turned into cubes, the faces of which are taken as representative grain areas (Tab. 2).

Figure 12

Temperatures of opening of grain boundaries, based on the P-T paths of the analyzed samples and on contour lines of volume change. The latter represent the increase (or decrease) in % from the volume at 25 °C ('room temperature') and 1 bar to the volume at different P-T conditions. The P-T paths are taken from figure 6. **(a)** Temperatures of grain boundary opening of Qz for samples (1) HH147B, (2) KR4717, (3) KR4874, (4a) KR5184X and (4b) KR5185X. The contour lines (black solid lines) are based on data given by Raz et al. (2002, table 3). For each sample, additional contour lines are determined for the 25th and 75th percentile of measurements of grain area and the median of grain-boundary opening width (stippled lines in different colors) (Tab. 2), based on linear interpolation between the contour lines given by Raz et al. (2002). The two intersections of the 25th and 75th percentile contour lines with the P-T path (dots) are projected on the T-abscissa (broken lines), indicating the range of opening temperature. **(b)** Temperature of grain boundary opening of Ol (forsterite; sample KR5329X1) and Pl (low albite; samples KR2745A and B). The contour lines (black solid lines) are solely related to Ol and based on data given by Katzura et al. (2009 – table 1). Additional contour lines are determined for the 25th and 75th percentile of measurements of grain area and the mean of grain-boundary opening width (stippled lines) (Tab. 2), based on linear interpolation between the contour lines given by Katzura et al. (2009). The two intersections of the 25^{th} and 75^{th} percentile contour lines with the P-T path (dots) are projected on the T-abscissa. For Pl, P-T data related to the 25^{th} and 75^{th} percentile of measurements of the grain area and for the median of opening width of the grain boundary (Tab. 3) are taken from Benusa et al. (2005) and Stewart and Limbach (1967) and projected from the P-T path on the T-abscissa.

Table 1

Statistical data of the analyzed grain boundaries and grain areas, which form the basis for figures 9, 11 and 12; and table 2. Measurements of boundary widths (asterisks) between Ol (forsterite) and Srp are more numerous than those of grain areas.

Table 2:

Volume changes of grains in the analyzed samples, based on median values and 25^{th} and 75^{th} percentiles given in table 1. Based on the measured area A, the grain volume V0 is calculated as cube except for samples KR2745A und KR2745B where grains are modelled as elongate cuboids. The volumes of these cuboids are turned into cubes leading to the recalculated grain areas (cube faces), in order to harmonize the calculation of the volume increase for all samples. For an estimate of limits of error or range of data scatter refer to figures 4 and 11.

Table 3:

Unit-cell volume (pressure) and molar volume (temperature) of low albite as functions of pressure and temperature along the retrograde P-T path of samples KR2745A and B. Pairs of pressure and temperature are taken from the retrograde P-T path. Underlined = original data from Benusa et al. (2005) (pressure) and Stewart and Limbach (1967) (temperature); *italics* = data generated by linear interpolation; bold = P-T conditions determined from the measured volume change related to the 25^{th} and 75^{th} percentiles of grain area and boundary width given in table 2.

Authors' contributions:

J.H. Kruhl and W.W. Schmahl designed the study. TEM measurements were performed by R. Wirth and SEM measurements by E. Griesshaber and J.H. Kruhl. The latter conducted the u-stage measurements. All authors discussed the results and contributed to the manuscript.

Revised Manuscript with Changes Marked

Click here to view linked References

Fracturing and widening of grain boundary networks in quartz, plagioclase and olivine crystal aggregates during exhumation at low P-T conditions

Jörn H. Kruhl[a*], Erika Griesshaber[a], Wolfgang W. Schmahl[a], Richard Wirth[b]

[a] Department of Earth and Environmental Sciences, Ludwig-Maximilians-Universität, 80333 Munich, Germany

[b] Helmholtz Centre Potsdam, GFZ German Research Centre for Geosciences, Potsdam, Germany

* Corresponding author, +498921804351

Jörn H. Kruhl	kruhl@tum.de
Erika Griesshaber	e.griesshaber@lrz.uni-muenchen.de
Wolfgang W. Schmahl	Wolfgang.W.Schmahl@lrz.uni-muenchen.de
Richard Wirth	wirth@gfz-potsdam.de

Abstract

Grain boundary networks of quartz, plagioclase and olivine crystal aggregates in metamorphic rocks have been investigated from the nanometer to the millimeter scale by polarized-light microscopy, SEM, and TEM. The studied materials show different grain sizes and experienced different retrograde P-T histories. The aggregates of quartz and plagioclase are traversed by networks of ~90% continuously open boundaries with µm-sized cavities along the boundaries or at triple junctions. The boundaries are up to ~500 nm wide open with typically parallel opposing grain faces. Olivine boundaries are filled with serpentine that does not replace olivine but fills the initially open space homogeneously and mostly with random orientation. For quartz there is no correlation between the crystallographic orientation of grain boundaries and their widths. Amongst all samples analyzed, a weak positive correlation exists between grain size and width of open grain boundaries. The application of measured volume changes and elasticity data from the literature to the cooling-decompression paths of the analyzed materials suggests that fracturing with subsequent widening of the grain boundaries starts at temperatures recognizably below the transition from crystal-plastic to brittle behavior of quartz, plagioclase and olivine but not only under surface conditions. The high

amount of open boundaries causes an extensive permeability.

Keywords

Open grain boundaries, SEM, TEM, quartz, plagioclase, olivine

1. Introduction

Grain and phase boundaries strongly influence physical properties of crystalline materials; such as strength, rheological behavior, resistance to corrosion, reactivity, conductivity, or permeability (Behrmann, 1985; Mainprice et al., 1993; Aust et al., 1994; Shimada et al., 2002; Frary and Schuh, 2005, and references therein; Nagurney et al., 2021; Freitag et al., 2022). They affect a variety of processes as for instance deformation, metamorphic reactions, metasomatism or weathering (Voll, 1960; White and White, 1981; Yardley, 1989; Delvigne, 1998; Mancktelow and Pennacchioni, 2004; Vernon, 2004; Bukovská et al., 2015). Although grain and phase boundaries are regarded as generally closed structures, early transmission electron microscopy (TEM) mostly on quartz illustrated voids and open sections along boundaries in crystal aggregates but could not address this phenomenon in depth, due to the limitations of instruments available at that time (White, 1976; Doukhan and Trepied, 1979; Bell and Wilson, 1981; Behrmann, 1985; Watson and Brenan, 1987; Hippertt, 1994; Hiraga et al., 1999; Duyster and Stöckhert, 2001). More recent scanning electron microscopy (SEM) and TEM on natural as well as experimentally treated material, the former mostly on broken surfaces of crystal aggregates, revealed the existence of nanometer-sized voids and open sections along grain boundaries and of tubular voids with crystallographically controlled 3D shapes along three-grains junctions (Mancktelow et al., 1998; Mancktelow and Pennacchioni, 2004; Schenk and Urai, 2004; Price et al., 2006; Schenk et al., 2006; Fusseis et al., 2009; Schmatz and Urai, 2011; Billia et al., 2013; Burnard et al., 2015; Freitag et al., 2022).

Recent TEM studies show that grain boundaries of quartz (Qz) and calcite (Cal) as well as phase boundaries of feldspars (Fsp), amphiboles (Amp), orthopyroxene (Opx) and clinopyroxenes (Cpx) (abbreviations of mineral names after Whitney and Evans, 2010) in metamorphic and magmatic rocks are generally several hundred nanometers wide and completely open or partly filled with secondary low-T minerals (Kruhl et al., 2013; Wirth et al., 2021). These investigations also hint at permeability of grain boundary networks in 3D and propose volume reduction due to cooling and decompression during exhumation as mechanism of cracking and widening of grain and phase boundaries. Recent SEM studies on Qz grain boundaries provide supporting data (Nagurney et al., 2021). However, the amount of available data is still very small and currently supplemented by numerical modelling only to a limited extend (Raghami et al., 2020). Consequently, the cracking and widening mechanism is not well understood and the question is not answered at which P-T-conditions grain and phase boundaries fracture, open and form connected networks that cause permeability for fluids on a larger scale. The answers will deepen our knowledge about physical properties of crystalline materials at surface conditions and different depths of the continental and oceanic crust. Beyond that, the answers will shape our views on various geological processes, such as weathering, fluid transport, reactivity, and behavior of crystalline material under different deformation conditions in nature and experiments.

Due to the high resolution methods required, the previous studies all examined only a small number of instances, and thus, statistically sound data sets on size, frequency and distribution of voids are missing, with few exceptions (Schmatz and Urai, 2011; Billia et al., 2013). The same is true for geometry, size and crystallographic orientation of open or partly open grain and phase boundaries. Therefore, knowledge about the origin, properties, occurrence and significance of these micro-scale fabrics is still limited.

Local observations and limited data sets always leave some doubt about the statistical significance of an observation and the validity of more general conclusions. Therefore, with the present work, using high-resolution SEM with additional polarized-light microscopy, we access larger data sets, cover larger volumes and observe open grain and phase boundaries and their connectivity on a larger scale. Our study objects are grain boundaries of quartz, plagioclase and olivine – all minerals with strongly anisotropic, well-known thermo-elastic properties. The analyzed samples experienced different maximum P-T conditions and different exhumation P-T paths, and contain a wide range of grain sizes. This allows investigating the effects of microfabrics and P-T variations on cracking and widening of grain boundaries.

2. Methods

Our investigations are based on polarized-light and Scanning Electron Microscopy (SEM). In addition, Transmission Electron Microscopy (TEM) was applied, based on focused ion beam (FIB) sample preparation. Crystallographic orientations of grains and grain boundaries were determined by universal stage and grain areas were measured on the basis of digitized grain boundaries and with the aid of the open source image analysis program *ImageJ* (https://imagej.net/).

TEM was carried out with a Tecnai F20 X- twin electron microscope with a Schottky field emitter as electron source and equipped with a Gatan Tridiem Imaging Filter GIF, a Fishione high-angle annular dark field (HAADF) detector operating at a camera length (330 mm), which allows Z-contrast plus diffraction contrast imaging, and an EDAX X-Ray analyzer. EDX analyses were performed in scanning transmission mode (STEM) to prevent beam damage. Typically, acquisition time was 60 s and bright field images were acquired as energy filtered images applying a 20 eV window to the zero loss peak. For Qz at lower magnification, images were generally acquired in the scanning transmission mode as HAADF images, thus reducing the irradiation damage considerably. FIB sample preparation (Wirth, 2009) does not produce any of the grain boundary features described in our study. This was already discussed in previous papers (Kruhl et al., 2013; Wirth et al., 2021) and is additionally based on the experience of more than 8,000 TEM foils sputtered with FIB from different materials and studied with TEM by one of the authors (RW).

Secondary electron and back scattered electron imaging was carried out on a Hitachi SU5000 field emission SEM. Thin section surfaces were coated with up to 12 nm of carbon or/and up to 8 nm of Pt/Pd.

Both TEM and SEM have advantages and disadvantages with respect to measuring open grain boundaries. In our investigations, TEM foils are cut perpendicular to planar grain boundary segments. Therefore, measured grain boundary thicknesses are not biased by observation geometry. Open boundaries of up to 15 nm width can be measured without problems (Wirth et al., 2021). Outbreaks or depressions around boundaries at the thin-section surface, due to grinding and polishing, are clearly visible (Fig. 1a, c) and do not affect the thickness measurements. On the basis of repeated measurements, the inaccuracy of measurements is estimated as only 5 nm (Wirth et al., 2021). On the other hand, the high effort of sample preparation and the small sizes of the foils (generally not larger than ca. 9 x 8 µm) strongly limit the amount of investigated material. The total length of grain and phase boundaries, recently studied and published (Kruhl et al., 2013; Wirth et al., 2021) adds up to ~600 µm.

In contrast, SEM can be applied to areas of thin-section size allowing measurement of a much higher number of grain boundaries and permitting investigation of grain boundary networks. Sample preparation requires comparatively low effort, although polishing needs caution. However, the accuracy of measurement is lower compared to TEM. (i) Boundaries are partly oblique to the thin-section surface and may show irregular margins. The cut-effect requires time-consuming corrections by measuring the inclinations of the grain boundaries, preferentially with the universal-stage. (ii) Fractures in the grain boundary network may lead to widening of boundaries and cause additional bias of the measured widths (Fig. 2). Such boundaries were not included in the measurements. Fractures can be recognized by two characteristics: They are clearly wider than the surrounding open boundaries and they may locally transect grains, as shown in figure 2. (iii) In contrast to TEM, grinding and polishing of the thin-section surface may lead to excavation of material at the open grain boundary down to a few µm, or to the rotation of µm-sized fragments into the open boundary. The frequency is controlled by the quality of grinding and polishing. Such excavations or fragments are only visible with larger magnifications and sharp images (Fig. 1b, d). They may bias the data by enlarging or reducing the widths of open grain boundaries measured at the thin-section surface. It can be excluded that the voids formed due to volume change during uplift. Firstly, there is a clear correlation with the quality of grinding and polishing. Secondly, the voids show curved surfaces typical for fracturing of quartz and are often closely related to fractures running away from the grain boundary. Thirdly, they can be never observed in TEM foils away from the thin section surface. Fourthly, cooling and decompression lead to gross volume reduction. Under such conditions there is no process or stress field imaginable, which could cause such voids.

It is also worth noting that the likelihood of such modification of the grain boundary width by grinding and polishing means that methods that probe the outer material topography, such as atomic force microscopy (AFM), can over- or underestimate the widths of open grain boundaries. In fact, each method that can be applied to study open grain boundaries has its own advantages and disadvantages in resolution, preparation artefacts and methodical bias of data, and thus it is advisable to apply different methods and obtain large datasets.

In general, measurements at lower magnifications – e.g. below a few thousand, depending on the quality of the image – may lead to overestimation of grain boundary widths. However, even at magnifications below 1,000 strongly oblique but open boundaries can be identified as open (Fig. 2b). With magnifications up to 10,000—50,000, as applied in our investigation, opening widths of boundaries not too strongly inclined, i.e. with angles against the thin section of more than 60-70°, can be measured down to ca. 20 nm.

We would like to point out that the measured width of an open or partially filled grain boundary does not necessarily represent the distance, by which the two opposite grains were shifted away from each other. This is illustrated best by TEM images of kinked boundaries (Fig. 3; Kruhl et al., 2013 – figure 4a; Wirth et al., 2021 – figure 1b). Without kinks the direction of opening in 2D cannot be determined with certainty. Consequently, all boundary widths, measured at TEM or SEM images, represent the component of displacement normal to the boundary.

The areas of investigation were selected in thin sections under the polarized-light microscope. Based on photomicrographs of these regions – with crossed polarizers and gypsum test plate for better differentiation – grains and grain boundaries were numbered and their coordinates determined. SEM images of boundaries and boundary networks were taken and the boundary widths determined directly in these images. The c-axes of neighboring Qz grains were measured with the aid of the universal stage together with the inclinations of grain boundaries against the thin section in order to correct the cut-effect. Grain areas were determined with the open source image analysis program *ImageJ*, based on digitized outlines of grains in photomicrographs. In this way, opening widths of grain boundaries could be related to areas and crystallographic orientations of neighboring grains. However, area measurements performed in 2D cuts through 3D grains lead to underestimation of grain sizes on a statistical basis. This has to be kept in mind when correlating grain size to other parameters, such as grain boundary width.

In total, widths of 604 grain boundaries were measured by SEM together with the adjoining grains (Tab. 1) at magnifications of generally 10,000 to 25,000, in certain cases up to 50,000. In each thin section the measured area of Qz and Pl aggregates covers several mm^2. Measurements on Ol cover the entire thin section, i.e., areas of ~1.5 cm^2. On a statistical basis, widths of open grain boundaries additionally measured with TEM in the same samples are in the same range as widths measured by SEM (Fig. 4).

3. Materials

Three minerals in eight samples and thirteen thin sections were analyzed by scanning and transmission electron microscopy (SEM and TEM): Qz in five samples, Pl in two samples, and Ol in one sample. The materials have different microfabrics and experienced a variation of exhumation P-T histories, covering greenschist to granulite facies conditions, contact and ultra-high-pressure metamorphism.

Sample HH147B is a deformed Qz vein from the Orune Schists of the late Variscan basement in eastern Sardinia (Italy). It consists of elongate, intensely deformed Qz grains with strong subgrain pattern and deep-lobate boundaries (Fig. 5a). These grains form new, small recrystallized grains. The vein is transected by late, open fractures. Maximum conditions of metamorphism of ~450-500 °C and ~0.55 GPa were followed by cooling and decompression (Helbing, 2003 – figures 5-3 and 5-12). These P-T conditions represent an average for the Orune Schists. The studied sample was collected from the southernmost, that is, upper part of the unit. Therefore, P-T conditions of ~400-450 °C and ~0.4-0.45 GPa are a realistic assumption (Fig. 6).

Sample KR4717 was collected in the central part of the Aar Massif (Central Alps, Switzerland), a late Variscan granitic intrusion. The location is a road cut ca. 3 km north of Andermatt. Qz, Pl, Kfs, Bt and Chl are the main constituents. Qz is recrystallized to ca. 100-300 µm large grains but mm-sized relics of magmatic Qz are present (Fig. 5b). During Alpine orogeny the sample experienced temperatures and pressures of up to ~420 °C and 0.28 GPa (Frey et al., 1980). A P-T path is not available for this part of the Alpine Lepontine metamorphism. However, based on a cooling P-T path of Qz in an extensional vein from the Aar Massif (Mullis, 1996), a P-T path for the studied sample can be inferred, which runs straight from maximum P-T to surface conditions (Fig. 6). The recrystallized grains are mostly free of internal deformation structures indicating static conditions during cooling and decompression.

Sample KR4874 comes from a quartzite layer in the contact aureole of the late Caledonian Ballachulish Igneous Complex (Scotland). It consists of up to 1 mm large, polygonal Qz grains with generally smaller Kfs grains and additional Kfs films along Qz grain boundaries (Fig. 5c). The lack of deformation features points to absence of deformation during and after contact metamorphism. Conditions of metamorphism and deformation of the contact aureole are discussed and summarized by Pattison and Voll (1991). The sample experienced a maximum of 655-670 °C and 0.3 GPa (Masch and Heuss-Aßbichler, 1991; Pattison, 1991) with subsequent isobaric cooling to ~250 °C. Maximum P-T conditions of regional metamorphism at the sample site are estimated ~450-550 °C and ~0.6 GPa (Fig. 6). For further details see Kruhl et al. (2013). In the past, this sample was analyzed by TEM, based on FIB sample preparation, resulting in 13 measurements of Qz grain boundaries (Kruhl et al., 2013). Here, we present 117 SEM measurements of opening widths of Qz grain boundaries and their correlation with grain size and crystallographic orientation of the boundaries.

Samples KR5184X and KR5185X were taken from pyrope (Prp) megablasts-bearing white schists in the Dora Maira Massif (Western Alps), at Case Tapina, Vallone di Gilba, and Case Ramello, south of Parigi, Valle di Po. At these localities, coesite (Coe) in rocks of the continental crust was first described (Chopin, 1984). In addition to Prp, the rocks consist mostly of phengite (Ph), Ky, talc (Tlc) and up to several hundred µm large Qz inverted from Coe (Fig. 5d). Starting with peak P-T conditions of more than 3.5 GPa and ~750-800 °C, the samples experienced nearly isothermal decompression, crossed the Coe-Qz transition at ~2.8 GPa and 750 °C and cooled to ~400 °C at ~0.5 GPa (Schertl et al., 1991). Then they followed a relatively straight P-T path to surface conditions (Fig. 6).

Samples KR2745A+B come from a pegmatite at Montescheno (Valle Antrona), ca. 3 km west of Villadossola (Val d'Ossola, Southern Alps, Italy), strongly deformed during Alpine (Lepontine) metamorphism at amphibolite facies conditions. Plagioclase completely recrystallized to ca. 150-200 µm large, mostly polygonal, slightly elongate grains (Fig. 5e) under dominantly static conditions indicating T of ~550 °C. This is based on correlations with grain sizes of recrystallized Pl in the south-western Lepontine heat dome (Altenberger et al., 1989) and in agreement with mineral zoning in the southwestern Lepontine Dome west of Val d'Ossola (Bousquet et al., 2004). The P-T development at the sample site is not well constrained. However, it can be inferred from the general P-T development in the southwestern Lepontine Dome (Borghi et al., 1996) that peak conditions of Lepontine metamorphism at ~550 °C and 0.35 GPa were followed by approximately constant cooling and decompression to surface conditions (Fig. 6).

Sample KR5329X1 is mm-sized peridotite from the western part of the Finero Ultramafic Complex, Variscan lower continental crust (Valle Cannobina, Southern Alps, Italy). In addition to Ol (forsterite), it contains Phl, Opx, Cpx, Amp and Chr (Fig. 5f). The rock experienced deformation under lowermost granulite facies conditions (Kruhl and Voll, 1976; Zingg, 1983); subsequent, late-Variscan cooling and decompression to lower greenschist facies conditions (Handy et al., 1999); and exhumation during the Alpine orogeny (Fig. 6).

4. Results

SEM imaging of grain boundaries in Qz aggregates at magnifications of up to 50,000 reveals characteristics of grain boundary networks as well as details at various locations along the boundaries. In most cases single grains are completely encapsulated by open boundaries, at least in 2D (Fig. 7a). Grain aggregates are traversed by networks of continuously open boundaries with µm-sized cavities along the boundaries or at triple junctions (Fig. 7b). The boundaries are several hundred nanometers wide with typically strictly parallel opposing grain faces (Figs. 7a, c and 8c) also clearly visible in TEM images (Figs. 1a, c and 3). They may be decorated with cavities, whereas subgrain boundaries are generally cavity-free (Figs. 7c, d and 8a). Often, cavities exhibit triangular shapes with one triangle apex away from the boundary, typical for dislocation-induced cavities (Billia et al., 2013; Kruhl et al., 2013).

Rarely, fracturing and opening of subgrain boundaries start at triple junctions with boundaries but typically fail after a short distance (Fig. 7d). Strong dissolution and precipitation lead to arrays of cavities encapsulating euhedral to subhedral crystal areas (Fig. 8a). Particularly large dissolution-precipitation cavities occur at triple junctions (Fig. 8b, c), with irregular or regular shapes and branches along the boundaries (Fig. 8b). Nearly all analyzed Qz and Pl grain boundaries are open (or filled with epoxy). Only in rare cases short sections of boundaries appear closed (Fig. 8b). In contrast, Ol boundaries in peridotite are filled with Srp, which does not replace Ol but fills the open space homogeneously and mostly with random orientation (Fig. 8d). A second stage of grain boundary fracturing and opening is indicated by open space between the Srp filling and the neighboring Ol. This space is generally smaller than the initial space between Ol grains (Fig. 9).

The widths of open Qz as well as Pl grain boundaries cover a range of up to ~500 nm, with median values of ~50 to ~200 nm, in one case around 200 nm (Fig. 9). Only the widths of the boundaries between up to several mm large Ol grains are in the range of several µm and Ol-Srp boundaries in the range of up to 1 µm. Most distributions are clearly left-asymmetric with median values smaller than the mean.

The c-axes of pairs of neighboring Qz grains were measured together with the crystallographic orientation of the boundary, that is, the grain boundary pole between them. The sum of the angles between the grain boundary pole and the two Qz c-axes provides a measure of the crystallographic orientation of the grain boundary in relation to both neighboring grains. A low total angle indicates a grain boundary pole close to the c-axes of both grains; a high total angle points to a grain boundary pole close to a-axes of both grains. No correlation exists between crystallographic orientation of grain boundaries and their widths for Qz in all analyzed four samples, exemplified for the two samples KR4874 and HH147B in Fig. 10.

Grain sizes of pairs of neighboring Qz grains were measured and the average area related to the width of the open boundary between the two grains. Again, nearly no correlation exists in all analyzed four samples, exemplified for sample KR4874 in Fig. 4. However, the relationship between grain area and width of open grain boundary shows a weak positive correlation amongst all analyzed samples (Fig. 11). This is true for the five Qz samples and specifically for samples KR5184X and KR5185X, which experienced the same retrograde P-T history after conversion of coesite to low-quartz (Fig. 6) but developed highly different grain sizes and grain boundary widths. Also Ol with its much larger grain sizes fits the correlation, whereas the widths of Pl grain boundaries show somewhat higher values than Qz grains of similar size. Even slightly higher grain sizes in 3D, due to the cut-effect, would not change this general relationship. The effect of temperature on grain-boundary width remains ambiguous. A sample with very high T-max (KR5185X) has similar Qz grain-boundary width than samples with low T-max (KR4717 and HH147B) or has clearly higher grain-boundary widths (KR5184X) or similar ones in comparison to a sample with lower T-max (KR4874).

The possible effect of the retrograde P-T path on the opening widths of the grain boundaries is examined (Fig. 12). The idea is that the present grain sizes together with the half volumes of the surrounding open boundaries (half, because of the contribution of both neighboring grains) represent the initial grain sizes at the P-T conditions of grain boundary fracturing and beginning widening. The difference between initial and present grain size, i.e. the percentage of volume change, depends on the elasticity data of the specific minerals. In the literature, the percentages of volume change are related to P-T conditions and can be plotted as contour lines in P-T diagrams. Consequently, fracturing and widening of grain boundaries start at P-T conditions, where these contour lines transect the P-T paths of the analyzed samples. P-T-related volume variation for Qz is given by Raz et al. (2002) and for Ol by Katsura et al. (2009). For Pl it can be estimated from the data of Steward and Limbach (1967) for temperature changes and Benusa et al. (2005) for pressure changes (Tab. 3). Based on these literature data, the contour lines of the 25th and 75th percentile of measurements of grain area and the median of grain-boundary opening width are determined for our samples. The determination scheme is given in table 2.

It should be kept in mind that, due to the cut-effect, the true 3D values of grain sizes are statistically slightly higher than the calculated ones. Accordingly, the true percentages of volume change are slightly lower than the calculated ones because the measured volume changes, that is, the true volumes of open boundaries are related to grain sizes which are statistically smaller than the true ones. For Qz, the volume percentage of open grain boundaries can be related to temperatures between ~300 °C and ~50 °C and pressures below ~0.35 GPa (Fig. 12a). For Ol, it can be related to temperatures between ~170 °C and ~85 °C and pressures below ~0.08 GPa (Fig. 12b). Pl shows slightly higher values: temperatures of ~330-210 °C at pressures of ~0.1-0.05 GPa (Fig. 12b, Tab. 3). However, the volume changes of Pl are given independently for T and P in the literature and the combined effect is accordingly slightly inaccurate. Other sources of inaccuracy must be considered: (i) the imprecision of the P-T paths of the different samples, even if it is limited for near surface conditions; (ii) especially for quartz the acute angles between the P-T paths and the contour lines of volume change, leading to larger T-shifts with small shifts of volume change.

5 Discussion

Grain boundaries of quartz, plagioclase and olivine and phase boundaries between olivine and serpentine from seven different samples have been measured by SEM and TEM. The grain boundaries of Qz and Pl are continuously open, mostly with constant width along the entire observable extension. Ol boundaries are nearly always filled with Srp. This means that also these boundaries were initially open. Even slightly open boundaries flatly inclined towards the section can be recognized as such under the applied high magnifications (Figs. 2 and 7a). In fact, directions of inclination can be determined and angles of inclination estimated and or precisely measured with the universal stage.

These observations show that most grains are completely separated in 2D (Figs. 2b and 7). Only few sections of boundaries are visible, which appear closed (Figs. 8b and 7c, d). Based on TEM measurements of 68 Qz grain boundaries, 33 published (Kruhl et al., 2013; Wirth et al., 2021) and 35 unpublished, the amount of open boundaries in Qz aggregates was estimated ~90 %, related to the total length of analyzed boundaries (Wirth et al., 2021). This value is confirmed by additional TEM measurements of grain and phase boundaries of Cal, Pl, Kfs, Crd, Sil, Srp, Amp, Opx, Cpx and Grt; 33 published (Wirth et al., 2021) and 18 unpublished. Closed sections can be clearly identified under HR-TEM. Based on a much larger data set, the present SEM investigations, too, confirm the value of ~90% total length of open grain boundaries, which should also hold for 3D. Such a high amount of open boundaries inevitably causes an extensive permeability. Consequently, the already observed connectivity of tubes along triple lines (White and White, 1981; Schenk and Urai, 2004) is complemented by a planar connectivity with accordingly increased permeability. Under which conditions this does occur will be discussed further below.

If ~90% of the grain and phase boundaries in rocks are open at the surface and in the uppermost part of the crust what holds the rocks together and ensures their strength? Firstly, after fracturing and widening the open boundaries are partially or totally filled with secondary minerals in the majority of rocks (Wirth et al., 2021). The boundaries between the fillings and the neighboring host grains are partially or totally closed. The fillings cause the cohesion of the rocks. Secondly, grain and phase boundaries are nearly always uneven. Their irregular geometry ranges from steps on the nanometer-scale to sutures of any shape and depth on the micrometer to millimeter-scale. They cause the strength of the rocks and guarantee that it is not possible to dismember a piece of rock easily even if grain and phase boundaries are totally open. Thirdly, the ~10% closed boundaries also contribute to the rock strength. However, currently the question about rock strength cannot be completely satisfactorily answered.

The extensive permeability allows access for larger amounts of fluids, if present. This may trigger dissolution-precipitation, specifically in Qz, already reported from various rocks (Watson and Brenan, 1987; Hippertt, 1994; Mancktelow et al., 1998; Mibe et al., 2003; Kruhl et al., 2013; Klevakina et al., 2014) and also leave imprints in the studied rock samples. Numerous mostly triangular cavities occur along open boundaries and at triple junctions (Figs. 1d; 7 and 8c, d) with crystallographically controlled faces (Fig. 8a). Such crystallographic control was also confirmed in previous studies (Mancktelow et al., 1998; Mancktelow and Pennacchioni, 2004; Billia et al., 2013; Kruhl et al., 2013; Wirth et al., 2021). The pyramidal shape and areal distribution of the cavities are a commonly presented feature in SEM investigations of broken surfaces of Qz crystal aggregates (Watson and Brenan, 1987; Mancktelow et al., 1998; Bestmann et al., 2011; Schmatz and Urai, 2011; Billia et al., 2013). These cavities were interpreted alternatively as (i) fluid inclusions along healed fractures (Hiraga et al., 1999), (ii) the result of grain boundary sliding (White, 1976; Behrmann, 1985; Mancktelow et al., 1998; Fusseis et al., 2009; Menegon et al., 2015), or (iii) accumulation of fluid during dynamic recrystallization (Mancktelow et al., 1998; Billia et al., 2013). Mancktelow and Pennacchioni (2004) notice that these cavities occur more frequently in 'wet' grain aggregates of a Qz-Fsp mylonite compared to 'dry' Qz aggregates. This is in agreement with our observation that grain boundaries in a late-Variscan Qz vein are strongly decorated with cavities of up to µm size (Fig. 7c, d) and show additional intensive dissolution features (Fig. 8a), although cavities are also present along grain boundaries in other samples. The interpretation of these cavities as dissolution pits generated by fluids in a permeable network of open grain and phase boundaries (Billia et al., 2013; Kruhl et al., 2013; Wirth et al., 2021) is backed by the observation that the cavities dominantly occur where dislocations or low angle boundaries meet open grain boundaries, i.e., at sites of increased solubility (Billa et al., 2013, Fig. 7a; Kruhl et al., 2013; Wirth et al., 2021, Fig. 9). In addition, variable occurrence of cavities may be caused by variable dissolubility at crystal faces of different crystallographic orientation (Benedová and Leichmann, 2016). Notably, dissolution pits are not present, or only in small numbers, along low-angle boundaries (Fig. 7c, d) and in aggregates of ultrafine Qz grains with almost entirely closed boundaries, where increased fluid flow cannot be expected (Bestmann et al., 2011, 2012). All this indicates that most dissolution cavities were generated during migration of fluids through open boundaries.

Ol grain boundaries are mostly filled with randomly oriented Srp (Fig. 8d), which neither grows at the expense of Ol nor as fibers perpendicular to the boundary typical of fiber veins (Ramsay and Huber, 1983; Passchier and Trouw, 2005, Chap. 6; Bons et al., 2012). It fills tubular dissolution cavities. Consequently, the boundaries were filled after initial opening. The Srp probably originates from a fluid infiltrating the open boundaries from larger depth.

The boundaries between Ol and Srp filling are mostly open (Fig. 8d). This indicates that the Ol grain aggregate did not cool, fracture, widen and fill with Srp under surface conditions but at elevated T, i.e., at a certain depth. This conclusion is supported by TEM observations of twofold opening of phase boundaries between sheet-silicate filling and surrounding grains of Qz, Amp and Px (Wirth et al., 2021 – Fig. 5, 8).

Kruhl et al. (2013) postulated that during exhumation Qz grain boundaries fracture and open due to cooling-related volume reduction below the transition from dominant crystal-plastic to brittle behavior of Qz, i.e., below ~300 °C (Voll, 1976; Stöckhert et al., 1999; Stipp et al., 2002), which is not balanced by decompression-related volume expansion. The strong P-T-related anisotropy of volume change (Ackermann and Sorrell, 1974; Levien et al., 1980; Kihara, 1990; Raz et al., 2002) leads to a larger width of grain boundaries perpendicular to Qz-<a> compared to grain boundaries perpendicular to Qz-[c]. The confining pressure telescopes the opening grain aggregate, so that boundaries perpendicular to Qz-[c] are preferentially closed while boundaries perpendicular to Qz-<a> remain partly open. At an amount of roughly 50% closed and 50% open boundaries the grain aggregate forms a stress-resistant framework that protects the still open boundaries of further closing (Kruhl et al., 2013). This model was initially backed by in total 19 TEM measurements of Qz grain boundary width and grain size, which show a weak correlation.

However, two observations indicate that the model cannot be true in detail. Firstly, as stated above, ~90% of the grain and phase boundaries are open in the range of up to several hundred nanometers. This is based on a much larger data set than the initial TEM investigation that led to the model. Secondly, grain boundaries perpendicular or at a high angle to Qz-<a> should be more widely open than boundaries at a high angle to Qz-[c]. However, a correlation between the crystallographic orientation of grain boundaries and their opening width does not exist in the analyzed Qz samples (Fig. 10). This does not necessarily argue against the concept that the anisotropic thermo-elasticity of Qz governs the opening of grain boundaries. A SEM study on a contact-metamorphic quartzite demonstrates that boundaries at high angles to Qz-<a> are statistically wider open than boundaries at high angles to Qz-[c] (Nagurney et al., 2021).

In general, the absence of a clear correlation in the analyzed quartz aggregates between the gap-width and the crystallographic orientation of the boundary may have different reasons. (i) Grain boundaries open at different times as suggested by 3D numerical modelling, combining contact mechanics and finite-element method (Raghami et al., 2020). This may lower the effect of anisotropic volume change. (ii) Grains may move relatively to each other during volume reduction under confining pressure. This may locally change grain boundary widths. Such movements have been observed under the TEM (Wirth et al., 2021 – Fig. 5A, 13) and are confirmed by 3D numerical modelling (Raghami et al., 2020). (iii) During volume reduction, the irregular shape of grains (Figs. 5 and 7) blocks their unimpeded movement and, therefore, reduces the effect of crystallography on the widening of grain boundaries. (iv) The variation of grain size, in combination with a low crystallographic preferred orientation of the quartz grains, may reduce the effect of the crystallographic orientation of the grain boundaries.

In each of the studied samples, the widths of open boundaries and the sizes of the bordering grains correlate only extremely weakly (Fig. 4). This at least partly results from the inaccurate size determination of grains of irregular shape and from the cut-effect that hampers inferring 3D sizes from 2D. In addition, as visible under the TEM as well as SEM, the grain aggregates may open along inter or intra-granular fractures (Figs. 2 and 5a,f), which may reduce the widening along neighboring grain boundaries. However, grain boundary widths and grain sizes correlate between the analyzed samples, which provide a much larger range of grain boundary width and grain size (Fig. 11). On a statistical basis, grain aggregates with larger grains have wider grain boundaries. This is true for Qz and specifically for the two samples KR5185X and KR5184X. They experienced the same maximum P-T conditions and the same retrograde P-T path but show clearly different grain boundary widths and grain sizes. Small grains are related to small grain boundary widths (KR5185X) and larger grains are related to larger grain boundary widths (KR5184X). The positive correlation between grain size and grain boundary width also holds if Qz, Pl and Ol are considered together. It is in agreement with the concept that the thermo-elastic properties of these minerals are mainly responsible for fracturing and widening of grain and phase boundaries.

Under which P-T-conditions do fracturing and widening take place? Principally, these processes can start as soon as cooling starts, i.e., at T between ~700 °C and ~400 °C for the analyzed minerals (Fig. 6). But such a scenario would require much larger grain boundary widths than measured, possible reduction by confining pressure not considered, and at least the occasional occurrence of higher-T fillings. However, up to now such fillings have not been observed, although low-T secondary minerals are widespread in grain and phase boundaries in a large variety of metamorphic and magmatic rocks (Wirth et al., 2021).

As a different approach, we compare the measured opening widths of the grain boundaries with the widths that would theoretically develop from fracturing and widening of the boundaries during cooling and decompression up to surface conditions (Tab. 2 and 3, Fig. 12). Such comparison results in P-T conditions of fracturing of grain boundaries with subsequent widening at ~300 to ~50 °C and up to ~0.35 GPa for Qz (Fig. 12a) and ~170 to ~85 °C and ~0.08 GPa for Ol (Fig. 12b).

Estimations for Pl suggest ~330 to ~210 °C and ~0.1-0.05 GPa (Fig. 12b). How realistic are these values? Given that grain sizes inferred from grain areas are generally slightly lower than the true ones, the estimated P-T values appear potentially even too high. In addition, inaccuracies are introduced by inaccurate determinations of grain areas, grain boundary widths and P-T paths. The small angles between the contour lines of cooling-decompression related volume change and the P-T paths, specifically for Qz, may lead to further inaccuracy. Independently, the estimated T and P may be too low if open boundaries were partly closed by the confining pressure during exhumation. However, this is contradicted by the observation that at least 90% of the grain boundaries are open and that only low-T minerals have been found so far as fillings of open grain boundaries (sheet silicate, chlorite, serpentine) and only in rare cases minerals that may form at lowermost greenschist facies conditions (biotite, actinolite) (Wirth et al., 2021). It is additionally contradicted by the observation that fibrous fillings of grain and phase boundaries are nearly never even slightly deformed (Fig. 8d; Wirth et al., 2021 – Fig. 6, 8, 12). On the other hand, opening under ambient conditions can be largely excluded due to (i) the occurrence of minerals like biotite and actinolite, and (ii) the observation that also phase boundaries between secondary, low-T minerals and the adjoining host grains fracture and widen. This indicates ongoing volume reduction after filling of open boundaries.

Furthermore, 3D grain-scale numerical modelling of grain boundary fracturing and widening in Qz grain aggregates shows that fracturing of Qz grain boundaries starts at ~220 °C, assuming that the thermo-elastic strain becomes operative below the transition from dominant crystal-plastic to brittle behavior of Qz, i.e., below ~300 °C (Raghami et al., 2020). This T-difference is related to the tensile yield strength of the boundaries, which has to be overcome. In this context, it is worth mentioning that Qz grain aggregates with grain sizes of only a few µm or below do not show considerable widening, if at all (Fitz Gerald et al., 2006; Bestmann et al., 2012).

In summary, independently of various uncertainties of measurements and T-estimations and based on observations and data sets available in the literature, it becomes clear that fracturing and widening of grain boundaries in the investigated grain aggregates of quartz, plagioclase and olivine take place under low T and P conditions. Such conditions are well below the transitions from crystal-plastic to brittle behavior of these minerals. Consequently, the experienced peak conditions of metamorphism or magma crystallization do not affect the fracturing and the widths of open or refilled grain boundaries.

6. Conclusions

Our investigation shows that a modern SEM is able to measure open grain and phase boundaries with sufficient precision and at the same time this method allows to obtain a data volume that is large enough for statistically sound conclusions. However, large magnifications are necessary, preferably more than five to ten thousand times. SEM bridges the gap between high-precision TEM measurements on small sample volumes and the relatively inaccurate measurements on large sample volumes with the polarized-light microscope. The combination of these methods allows the investigation of grain and phase boundaries and their networks from the nanometer to the millimeter scale, i.e., over about 6-7 orders of magnitude.

Totally or partially open grain and phase boundaries at higher crustal levels and at the surface cause permeability, provide the opportunity for extensive fluid flow and, consequently, affect physical properties of rocks and a variety of geological processes. In addition, it should be tested if open boundaries also occur in other crystalline materials, such as ceramics or metals, with similar effects on material properties and processes.

The results of our investigations neither indicate nor disprove the occurrence of networks of totally or partially open grain and phase boundaries under higher P-T conditions, e.g., at mid-crustal levels. Quartz boundaries are most probably not open at such depth but grain boundaries of other minerals, such as feldspars, pyroxenes or amphiboles, with a much higher transition temperature from crystal-plastic to brittle behavior may be open. The investigations to date are still too limited for such statements and studies on a larger variety of rocks with different mineralogy and different P-T histories are necessary. Furthermore, data sets measured by a wide variety of methods need to be acquired and compared.

Acknowledgements

We gratefully acknowledge the help of Anja Schreiber, who prepared the TEM foils with FIB. Thanks are due to Günter Buntebarth for providing a sample from the Ballachulish contact aureole, to Peter Gille for providing access to and help with a high-precision saw, to Guntram Jordan for a useful discussion, and to John Platt, an anonymous reviewer and Virginia Toy for detailed and helpful reviews. The investigations were financially supported by the German Research Council (DFG) under grant SCHM390/17-1 / KR691/36-1.

References

Altenberger, U., Hamm, N., Kruhl, J.H., 1987. Movements and metamorphism north of the Insubric Line between Val Loana and Val d'Ossola, N.Italy. Jahrbuch Geologische Bundesanstalt Wien 130(4), 365-374.

Ackermann, R.J. and Sorrell, C.A., 1974. Thermal expansion and the high-low transformation in Quartz. I. High-temperature X-ray studies. Journal of Applied Crystallography 7, 461-467.

Aust, K.T., Erb, U., Palumbo, G., 1994. Interface control for resistance to intergranular cracking. Materials Science and Engineering A 176, 329-334.

Behrmann, J.H., 1985. Crystal plasticity and superplasticity in quartzite: a natural example. Tectonophysics 115, 101-129.

Bell, I.A. and Wilson, C.J.L., 1981. Deformation of biotite and muscovite: TEM microstructure and deformation model. Tectonophysics 78, 201-228.

Benedová, Š. and Leichmann, J., 2016. Experimental study of anisotropy of quartz dissolution and its role in fluid migration in rocks. Acta Geodynamica et Geomaterialia 13(2), 193–200, https://doi.org/10.13168/AGG.2016.0001.

Benusa, M.D., Angel, R.J., Ross, N.L. (2005). Compression of albite, NaAlSi3O8. American Mineralogist 90, 1115-1120, https://doi.org/10.2138/am.2005.1805.

Bestmann, M., Pennacchioni, G., Frank, G., Göken, M., de Wall, H., 2011. Pseudotachylyte in muscovite-bearing quartzite: Coseismic friction-induced melting and plastic deformation of quartz. Journal of Structural Geology 33, 169-186, https://doi.org/10.1016/j.jsg.2010.10.009.

Bestmann, M., Pennacchioni, G., Nielsen, S., Göken, M., de Wall, H., 2012. Deformation and ultrafine dynamic recrystallization of quartz in pseudotachylyte-bearing brittle faults: A matter of a few seconds. Journal of Structural Geology 38, 21-38, https://doi.org/10.1016/j.jsg.2011.10.001.

Billia, M.A., Timms, N.E., Toy, V.G., Hart, R.D., Prior, D.J., 2013. Grain boundary dissolution porosity in quartzofeldspathic ultramylonites: Implications for permeability enhancement and weakening of mid-crustal shear zones. Journal of Structural Geology 53, 2-14, http://dx.doi.org/10.1016/j.jsg.2013.05.004.

Borghi, A., Compagnoni, R., Sandrone, C., 1996. Composite P-T paths in the Internal Penninic Massifs of the Western Alps: Petrological constraints to their thermo-mechanical evolution. Eclogae geologicae Helvetiae 89(1), 345-367.

Bohlen, S.R., Montana, A., Kerrick, D.M., 1991. Precise determinations of the equilibria kyanite - sillimanite and kyanite - andalusite and a revised triple point for Al_2SiO_5 polymorphs. American Mineralogist 76(3-4), 677-680.

Bons, P.D., Elburg, M.A. Gomez-Rivas, E., 2012. A review of the formation of tectonic veins and their microstructures. Journal of Structural Geology 43, 33-62, http://dx.doi.org/10.1016/j.jsg.2012.07.005.

Bousquet, R., Engi, M., Gosso, G., Oberhänsli, R., Berger, A., Spalla, M.I., Zucali, M., Goffè, B., 2004. Explanatory notes to the map: metamorphic structures of the Alps – transition from the Western to the Central Alps. Mitteilungen der Österreichischen Mineralogischen Gesellschaft 149, 145-156.

Bukovská, Z., Wirth, R., Morales, L.F., 2015. Pressure solution in rocks: focused ion beam / transmission electron microscopy study on orthogneiss from South Armorican Shear Zone, France. Contributions to Mineralogy and Petrology 170:31, https://doi.org/10.1007/s00410-015-1186-8.

Burnard, P.G., Demouchy, S., Delon, R., Arnaud, N.O., Marrocchi, Y., Cordier, P., Addad, A., 2015. The role of grain boundaries in the storage and transport of noble gases in the mantle. Earth and Planetary Science Letters 430, 260–270, http://doi.org/10.1016/j.epsl.2015.08.024.

Chopin, C., 1984. Coesite and pure pyrope in high-grade blueschists of the Western Alps: a first record and some consequences. Contributions to Mineralogy and Petrology 86, 107-118.

Delvigne, J. E., 1998. Atlas of micromorphology of mineral alteration and weathering. The Canadian Mineralogist, Special Publication 3. Mineralogical Association of Canada, 494 pp.

Doukhan, J.-C., Trepied, L., 1979. Plasticity of quartz: crystallographic models and T.E.M. Observations. Bulletin de minéralogie 102, 138-147.

Duyster, J., Stöckhert, B., 2001. Grain boundary energies in olivine derived from natural microstructures. Contributions to Mineralogy and Petrology 140, 567-576, https://doi.org/10.1007/s004100000200.

Fitz Gerald, J.D., Mancktelow, N.S., Pennacchioni, G., Kunze, K., 2006. Ultrafine-grained quartz mylonites from high-grade shear zones: Evidence for strong dry middle to lower crust. Geology 34(5), 369–372, https://doi.org/10.1130/G22099.1.

Frary, M., Schuh, C.A., 2005. Grain boundary networks: scaling laws, preferred cluster structure, and their implications for grain boundary engineering. Acta Materialia 53, 4323-4335.

Freitag, S., Klaver, J., Malai, I.S., Klitzsch, N., Urai, J.L., Stollhofen, H., Bauer, W., Schmatz, J., 2022. Petrophysical characterization, BIB-SEM imaging, and permeability models of tight carbonates from the Upper Jurassic (Malm ß), SE Germany. Geothermal Energy 10:30, https://doi.org/10.1186/s40517-022-00239-x

Frey, M., Bucher, K., Frank, E., 1980. Alpine metamorphism along the geotraverse Basel-Chiasso: a review. Eclogae Geologicae Helvetiae 73(2), 527-546.

Frey, M., Ferreiro Mählmann, R. (1999). Alpine metamorphism of the Central Alps. Schweizerische mineralogische und petrographische Mitteilungen 79, 135-154.

Fusseis, F., Regenauer-Lieb, K., Liu, J., Hough, R.M., De Carlo, F., 2009. Creep cavitation can establish a dynamic granular fluid pump in ductile shear zones. Nature Letters 459, https://doi.org/10.1038/nature08051.

Gross, A.F.K., Van Heege, J.P.T., 1973. The high-low quartz transition up to 10 kb pressure. Journal of Geology 81, 717-724.

Handy, M.R., Franz, L., Heller, F., Janott, B., Zurbrigg, R., 1999. Multistage accretion and exhumation of the continental crust (Ivrea crustal section, Italy and Switzerland). Tectonics 18(6), 1154-1177.

Helbing, H., 2003. No suture in the Sardinian Variscides: a structural, petrological, and geochronological analysis. Tübinger Geowissenschaftliche Arbeiten, Reihe A 68, 1–190, http://w210.ub.uni-tuebingen.de/dbt/

Hippertt, J.F., 1994. Microstructures and c-axis fabrics indicative of quartz dissolution in sheared quartzites and phyllonites. Tectonophysics 229, 141-163.

Hiraga, T., Nagase, T., Akizuki, M., 1999. The structure of grain boundaries in granite origin ultramylonite studied by high-resolution electron microscopy. Physics and Chemistry of Minerals 26(8), 617–623, https://doi.org/10.1007/s002690050.

Hovis, G.L., Medford, E., Conclon, M., Tether, A., Romanovski, A., 2010. Principles of thermal expansion in the feldspar system. American Mineralogist 95, 1060–1068, https://doi.org/10.2138/am.2010.3484

Huang, W.L., Wyllie, P.J., 1981. Phase relationship of S-type granite with H_2O to 35 Kbar: muscovite granite from Harney Peak, South Dakota. Journal of Geophysical Research 86(B11), 1015–1029.

Katsura, T., Shatskiy, A., Geeth, M.A., Manthilake, M, Zhai, S., Fukuia, H., Yamazaki, D., Matsuzaki, T., Yoneda, A., Ito, E., Kuwata, A., Ueda, A., Nozawa, A., Funakoshi, K.-I., 2009. Thermal expansion of forsterite at high pressures determined by in situ X-ray diffraction: The adiabatic geotherm in the upper mantle. Physics of the Earth and Planetary Interiors 174, 86–92, https://doi.org/10.1016/j.pepi.2008.08.002.

Kerrick, D.M., 1968. Experiments on the upper stability limit of pyrophyllite at 1.8 kilobars and 3.9 kilobars water pressure. American Journal of Science 266(3), 204-214. https://doi.org/10.2475/ajs.266.3.204

Kihara, K., 1990. An X-ray study of the temperature dependence of the quartz structure. European Journal of Mineralogy 2(1), 63-77.

Klevakina, K., Renner, J., Doltsinis, N., Adeagbo, W., 2014. Transport processes at quartz–water interfaces: constraints from hydrothermal grooving experiments. Solid Earth 5, 883–899, https://doi.org/10.5194/se-5-883-2014

Kruhl, J.H., 1993. The P-T-d development at the basement-cover boundary in the north-eastern Tauern Window (Eastern Alps): Alpine continental collision. Journal of metamorphic Geology 11(1), 31-47.

Kruhl, J.H., Voll, G., 1976. Fabrics and Metamorphism from the Monte Rosa Root Zone into the Ivrea Zone near Finero, Southern Margin of the Alps. Schweizerische mineralogische und petrographische Mitteilungen 56, 627-633.

Kruhl, J.H., Wirth, R., Morales, L.F.G., 2013. Quartz grain boundaries as fluid pathways in metamorphic rocks. Journal of Geophysical Research Solid Earth 118(5), 1-11. https://doi.org/10.1002/jgrb.50099.

Levien, L., Prewitt, C.T., Weidner, D.J., 1980. Structure and elastic properties of quartz at pressure. American Mineralogist 65(9-10), 920-930.

Mainprice, D., Lloyd, G.E., Casey, M. (1993). Individual orientation measurements in quartz polycrystals – advantages and limitations for texture and petrophysical property determinations. Journal of Structural Geology 15, 1169-1187.

Mancktelow, N.S, Grujic, D., Johnson, E.L. (1998). An SEM study of porosity and grain boundary microstructure in quartz mylonites, Simplon Fault Zone, Central Alps. Contributions to Mineralogy and Petrology 131(1), 71-85.

Mancktelow, N.S., Pennacchioni, G., 2004. The influence of grain boundary fluids on the microstructure of quartz-feldspar mylonites. Journal of Structural Geology 26(1), 47-69.

Masch, L., Heuss-Aßbichler, S., 1991. Decarbonation reaction mechanisms of carbonate rocks: a comparison between the thermoaureoles of Ballachulish and Monzoni (N. Italy). In: Voll, G. et al. (Eds), Equilibrium and Kinetics in Contact Metamorphism. The Ballachulish Igneous Complex and Its Aureole, Springer, Berlin/Heidelberg/New York, 229–249.

Menegon, L., Fusseis, F., Stünitz, H., Xiao, X., 2015. Creep cavitation bands control porosity and fluid flow in lower crustal shear zones. Geology 43(3), 227–230, https://doi.org/10.1130/G36307.1.

Mibe, K., Yoshino, T., Ono, S., Yasuda, A., Fujii, T., 2003. Connectivity of aqueous fluid in eclogite and its implications for fluid migration in the Earth's interior. Journal of Geophysical Research 108(B6), 2295, https://doi.org/10.1029/2002JB001960.

Mullis, J., 1996. P-T-t path of quartz formation in extensional veins of the Central Alps. Schweizerische mineralogische und petrographische Mitteilungen 76(2), 159-164.

Nagurney, A.B., Caddick, M.J., Law, R.D., Ross, N.L., Kruckenberg, S.C., 2021. Crystallographically controlled void space at grain boundaries in the Harkless quartzite. Journal of Structural Geology 143, https://doi.org/10.1016/j.jsg.2020.104235.

Nicolas, A., Poirier, J.-P., 1976. Crystalline Plasticity and Solid State Flow in Metamorphic Rocks. Wiley, New York.

Passchier, C.W., Trouw, R.A.J., 2005. Microtectonics. 2nd edition, Springer, Berlin/Heidelberg/New York.

Pattison, D.R.M., 1991. P-T-a(H2O) conditions in the thermal aureole. In: Voll, G. et al. (Eds.), Equilibrium and Kinetics in Contact Metamorphism. The Ballachulish Igneous Complex and Its Aureole. Springer, Berlin/Heidelberg/New York, 327–350.

Pattison, D.R.M., Voll, G., 1991. Regional geology of the Ballachulish area. In: Voll, G. et al. (Eds.), Equilibrium and Kinetics in Contact Metamorphism. The Ballachulish Igneous Complex and Its Aureole. Springer, Berlin/Heidelberg/New York, 19–36.

Price, J.D., Wark, D.A., Watson, E.B., Smith, A.M., 2006. Grain-scale permeabilities of faceted polycrystalline aggregates. Geofluids 6(4), 302–318, doi:10.1111/j.1468-8123.2006.00149.x.

Raghami, E., Schrank, C., Kruhl, J.H., 2020. 3D modelling of the effect of thermal-elastic stress on grain-boundary opening in quartz grain aggregates. Tectonophysics 774, 1-13, https://doi.org/10.1016/j.tecto.2019.228242.

Ramsay, J.G., Huber, M.I., 1983. The Techniques of Modern Structural Geology. Vol. 1: Strain Analysis. Academic Press, Inc., London.

Raz, U., Girsperger, S., Thompson, A.B., 2002. Thermal expansion, compressibility and volumetric changes of quartz obtained by single crystal dilatometry to 700°C and 3.5 kilobars (0.35 GPa). Schweizerische mineralogische und petrographische Mitteilungen 82(3), 561–574, http://doi.org/10.5169/seals-62381.

Schenk, O., Urai, J.L., 2004. Microstructural evolution and grain boundary structure during static recrystallization in synthetic polycrystals of Sodium Chloride containing saturated brine. Contributions to Mineralogy and Petrology 146(6), 671–682, doi:10.1007/s00410-003-0522-6.

Schenk, O., Urai, J.L., Piazolo, S., 2006. Structure of grain boundaries in wet, synthetic polycrystalline, statically recrystallizing halite – evidence from cryo-SEM observations. Geofluids 6, 93–104.

Schertl, H.-P., Schreyer, W., Chopin, C., 1991. The pyrope-coesite rocks and their country rocks at Parigi, Dora Maira Massif, Western Alps: detailed petrography, mineral chemistry and PT-path. Contributions to Mineralogy and Petrology 108, 1–21.

Schmatz, J., Urai, J.L., 2011. The interaction of migrating grain boundaries and fluid inclusions in naturally deformed quartz: A case study of a folded and partly recrystallized quartz vein from the Hunsrück Slate, Germany. Journal of Structural Geology 33, 468-480, https://doi.org/10.1016/j.jsg.2010.12.010.

Shimada, M., Kokawa, H., Wang, Z.J., Sato, Y.S., Karibe, I., 2002: Optimization of grain boundary character distribution for intergranular corrosion resistant 304 stainless steel by twin-induced grain boundary engineering. Acta Materialia 50, 2331-2341.

Stewart, D.B., von Limbach, D., 1967. Thermal expansion of low and high albite. The American Mineralogist 52, 389-413.

Stipp, M., Stünitz, H., Heilbronner, R., Schmid, S.M., 2002. The eastern Tonale fault zone: A 'natural laboratory' for crystal plastic deformation of quartz over a temperature range from 250 to 700 °C. Journal of Structural Geology 24(12), 1861–1884, https://doi.org/10.1016/S0191-8141(02)00035-4.

Stöckhert, B., Brix, M.R., Kleinschrodt, R., Hurford, A.J., Wirth, R., 1999. Thermochronometry and microstructures of quartz – a comparison with experimental flow laws and predictions on the temperature of the brittle-plastic transition. Journal of Structural Geology 21, 351-369.

Tullis, J., 1983. Deformation of feldspars. Reviews in Mineralogy 2, 297-323.

Vernon, R.H., 2004. A practical guide to rock microstructure. Cambridge University Press, 594 pp.

Voll, G., 1960. New work on petrofabrics. Liverpool and Manchester Geological Journal 2, 503-567.

Voll, G., 1976. Recrystallization of quartz, biotite and feldspars from Erstfeld to the Leventina Nappe, Swiss Alps, and its geological significance. Schweizerische mineralogische und petrographische Mitteilungen 56, 641-647.

Watson, E.B., Brenan, J.M., 1987. Fluids in the lithosphere, 1. Experimentally-determined wetting characteristics of CO_2-H_2O fluids and their implications for fluid transport, host-rock physical properties, and fluid inclusion formation. Earth and Planetary Science Letters 85, 497-515.

White, S., 1976. The role of dislocation processes during tectonic deformations, with particular reference to quartz. In: Strens, R.J. (Ed.), The Physics and Chemistry of Minerals. Wiley-Interscience, London, 75-91.

White, J.C., White, S.H., 1981. On the structure of grain boundaries in tectonites. Tectonophysics 78, 613-628.

Whitney, D., Evans, D.W., 2010. Abbreviations for names of rock-forming minerals. American Mineralogist 95, 185–187, https://doi.org/10.2138/am.2010.3371.

Wirth, R., 2009. Focused Ion Beam (FIB) combined with SEM and TEM: Advanced analytical tools for studies of chemical composition, microstructure and crystal structure in geomaterials on a nanometre scale. Chemical Geology 261, 217–229, https://doi.org/10.1016/j.chemgeo.2008.05.019.

Wirth, R., Kruhl, J.H., Morales, L.F.G., Schreiber, A., 2021. Partially open grain and phase boundaries as fluid pathways in magmatic and metamorphic rocks. Journal of Metamorphic Geology 40, 65-87, https://doi.org/10.1111/jmg.12610.

Yardley, B.W.D., 1989. An introduction to metamorphic petrology. Longman Group, 248 pp.

Zingg, A., 1983. The Ivrea and Strona-Ceneri Zones (Southern Alps, Ticino and N-Italy) – A Review. Schweizerische mineralogische und petrographische Mitteilungen 63, 361-392.

Captions

Figure 1

TEM and SEM images of Qz grain boundaries. **(a)** HAADF TEM image of an open Qz grain boundary from a jadeite quartzite (Shuanghe, Dabie–Sulu Belt, Central Eastern China). The light band (Pt) is a protective layer of platinum covering the thin-section surface prior to FIB milling. A small depression occurs where the grain boundary meets the thin-section surface. Sample RP11, foil 3344. **(b)** SEM image of a Qz grain boundary. Irregular depressions on both sides along the boundary were generated by grinding and polishing of the thin section. The open boundary with sharp parallel crystal faces on both sides is clearly visible (arrow). Locally, relics of epoxy cover the boundary margins (double arrows). Quartzite from the contact aureole of the late Caledonian Ballachulish Igneous Complex (Scotland). Sample KR4874. **(c)** HAADF TEM image of an open Qz grain boundary from the same sample. Modified figure 2b from Kruhl et al. (2013). The light band (Pt) is a protective layer of platinum covering the thin-section surface prior to FIB milling. A small grain fragment (white arrow) is rotated into the open grain boundary (curved black arrow), probably during thin-section polishing. Platinum fills the open space at the tip of the grain boundary (double arrow). Sample KR4874, foil 2075. **(d)** SEM image of three open Qz grain boundaries (black arrows) and their triple junction. Along the boundaries the grains are partly fragmented (x) and excavated, due to grinding during thin-section preparation. Excavation is particularly large at the triple junction, where the boundaries form a triangular cavity (white arrow). Sample HH147B-3; Qz vein in the late Variscan basement of the Baronie (eastern Sardinia, Italy).

Figure 2

Polarized-light photomicrograph with crossed polarizers and gypsum test plate **(a)** and SEM (BSE mode) image **(b)** of a network of continuously open grain boundaries in an aggregate of polygonal Pl grains. Sample KR2745A-1, section perpendicular to foliation and lineation. Inspections at magnifications of up to 30k show that the boundaries are open even if appearing closed at lower magnifications in the polarized-light image or the SEM image (short open arrows). They may be widened by fractures that locally transect grains (long arrows). Flatly dipping open boundaries lead to excavations at the thin-section surface (asterisks). Tiny spots are mostly due to grinding and polishing.

Figure 3

TEM images of open, kinked Qz grain boundaries. **(a)** HAADF TEM image of a Qz grain boundary in Cambrian quartzite („Pipe Rock“) from the Moine Thrust Zone at Loch Assynt (Scotland). Sample KR4970-1; foil 6104. The kinks of the open boundary between the perfectly matching faces of the opposite grains Qz1 and Qz2 indicate displacement of the grains by ~60 nm parallel to the horizontal white lines. The longer sections of the boundary in the lower left and upper right parts of the image are only ~30 nm wide (thick, short white line). Numerous subgrain boundaries are interspersed throughout the grains (white arrows). Where they meet the open boundary, cone-shaped euhedral dissolution cavities occur (double arrow). Euhedral black spots represent fluid inclusions. **(b)** TEM bright-field image of a Qz grain boundary in hydrothermal Qz from the 'Pfahl' (Bavarian Forest, Germany). Sample KR5095A-3; foil 5840. The kinks of the open boundary between the perfectly matching faces of the opposite grains Qz1 and Qz2 indicate displacement of the grains by ~260 nm parallel to the black lines. The widths of the different boundary sections of ~230 nm and 145 nm (black double lines) are clearly lower. The white double arrow points to a cone-shaped dissolution cavity where a dislocation meets the open boundary.

Figure 4

Relationship between grain area and width of open Qz grain boundary, based on SEM and TEM measurements. The latter are taken from Kruhl et al. (2013) and recalculated for grain area instead of grain diameter. For the one measurement outside the diagram the grain area is given. Broken lines mark the 25th and 75th percentiles for grain area and boundary width. Sample KR4874; quartzite from the contact aureole of the late Caledonian Ballachulish Igneous Complex (Scotland).

Figure 5

Photomicrographs of the studied samples; all with crossed polarizers and gypsum plate inserted for better distinction between the different grains. **(a)** Sample HH147B-5: Qz vein from the late Variscan basement of the Baronie (eastern Sardinia, Italy). Long grain axes represent the main regional foliation. Strongly lobate grain boundaries result from deformation under greenschist facies conditions and, locally, form a second generation of small recrystallized grains (arrows). A network of partly open cracks transects the material (double arrows). **(b)** Sample KR4717: late Variscan granite (Aar Massif, Central Alps, Switzerland) deformed and recrystallized under lower greenschist facies conditions. Relics of magmatic Qz with subgrain boundaries are preserved (X). Magmatic Pl shows strong alteration (saussuritization) due to prograde Alpine ('Lepontine') metamorphism. **(c)** Sample KR4874: quartzite from the contact aureole of the late Caledonian Ballachulish Igneous Complex (Scotland) with up to 1 mm large, roughly polygonal Qz and typically smaller Kfs. Recrystallized Qz from regional greenschist facies deformation and metamorphism coarsened during contact metamorphism. Kfs forms thin layers along Qz grain boundaries (arrows). **(d)** Sample KR5185X: polygonal Qz grain aggregate in a white schist from the Dora Maira Massif at (Case Ramello/Parigi, Valle di Po, and Case Tapina, Vallone di Gilba, Western Alps). In addition to Prp-megablasts and Qz, white mica (Ph) and Ky are frequent. The photomicrograph is also representative of sample KR5184X. **(e)** Sample KR2745B-3x: pegmatite from the southwestern Lepontine heat dome (Western Alps) deformed under lower amphibolite-facies conditions; aggregate of roughly polygonal, weakly elongate, recrystallized Pl grains (albite); section parallel to the main regional foliation. The long grain axes represent the lineation parallel to the short side of the image. **(f)** Sample KR5329X1: phlogopite peridotite from the Finero Ultramafic Complex, Variscan lower continental crust, Southern Alps (Valle Cannobina, Northern Italy). In addition to Ol (forsterite) and Phl, the rock contains partly euhedral Chr (black) and Cpx.

Figure 6

P-T paths of the investigated samples. Stability fields of Al_2SiO_5 polymorphs after Bohlen et al. (1991); upper stability limit of pyrophyllite (Pyp) after Kerrick (1968); wet granite solidus (wgs) after Huang and Wyllie (1981); low–high quartz transition (L/H) after Gross and Van Heege (1971);

approximate temperature threshold for dislocation creep (‘brittle-ductile transition’; Nicolas and Poirier, 1976) of various minerals, equivalent to recrystallization temperatures, with an uncertainty of ±10–15°C: Qz (Voll, 1976; Stöckhert et al., 1999; Stipp et al., 2002), Fsp (Pl and Kfs) (Voll, 1976; Tullis, 1983; Altenberger et al., 1987; Kruhl, 1993). (1) Sample HH147B, Baronie (Eastern Sardinia, Italy); (2) sample KR4717, Aar Massif (Central Alps, Switzerland); (3) sample KR4874, contact aureole of the Ballachulish Igneous Complex (Scotland); (4) samples KR5184X and KR5185X, Dora Maira Massif (Vallone di Gilba and Valle di Po, Western Alps, Italy); (5) samples KR2745A and B, Valle Antrona, Western Alps (Italy); (6) sample KR5329X1, Valle Cannobina (Western Alps, Italy).

Figure 7

SEM images of open Qz grain boundaries. **(a)** 20-30 μm sized grain completely encapsulated by up to 100 nm wide open boundaries. Excavated domains along the boundaries (arrows) are due to thin-section preparation. Cavities at a triple junction (double arrow) arise from dissolution-precipitation. BSE image; sample HH147B-8; Qz vein from the Orune Schists, Baronie (Sardinia, Italy). **(b)** Network of completely open boundaries in an aggregate of polygonal grains of recrystallized Qz. White arrows point to dissolution-precipitation related cavities along the boundaries and at triple junctions. SE image; sample KR4717; meta-granite, Aar Massif (Central Alps, Switzerland). **(c)** Continuously open Qz boundaries, locally with healed boundaries with cavities (short, thick, open arrow). The open boundaries are decorated with 1-2 μm large cavities (short arrows), whereas the numerous subgrain boundaries are generally cavity-free. The grains contain μm-sized probably primary inclusions. Healing of cracks led to arrays of inclusions (double arrows). BSE image; sample HH147B-5; Qz vein from the Orune Schists, Baronie (Sardinia, Italy). **(d)** Continuously open boundaries between polygonal Qz grains, locally with dissolution-precipitation cavities (short arrows). The subgrain boundaries (asterisk) are almost completely cavity-free. Incomplete opening from triple junctions along subgrain boundaries rarely occurs (double arrows). BSE image; sample HH147B-3; Qz vein from the Orune Schists, Baronie (Sardinia, Italy).

Figure 8

SEM images of open Qz and Ol grain boundaries. **(a)** Qz boundary with numerous, several μm-large cavities. Euhedral to subhedral crystal fragments (x) are shaped by dissolution and precipitation. Subgrain boundaries (arrows) are nearly free of cavities. BSE image; sample HH147B3; Qz vein from the Orune Schists, Baronie (Sardinia, Italy). **(b)** Several µm-sized dissolution-precipitation cavities at a triple junction (x) and along Qz grain boundaries (arrows). A section of the boundary appears closed on the thin-section surface (double arrow). SE image; sample KR4874-3; quartzite from the contact of the Ballachulish Complex (Scotland). **(c)** Junction of three 200-250 nm thick, open Qz grain boundaries. Opposing grain faces are mostly parallel except dissolved parts of grains marked by broken lines. Grain boundary kinks indicate directions of opening (double arrows). The boundaries are mostly filled with epoxy (whitish, grainy material). SE image; sample KR4874-2. **(d)** Approx. 4 µm thick boundary between two Ol grains, filled with serpentine (Srp), determined by TEM EDX. Srp is randomly oriented as shown by its spotty appearance. Short, thick arrow indicates tubular dissolution cavity filled with Srp. Several hundred nm-wide stripes of open space (black) occur between Srp and both neighboring Ol grains. Conical dissolution-precipitation cavities generated prior to Srp-filling indicate opening oblique to the Srp-Ol boundary (white arrows). Asterisks mark excavations due to sample preparation. BSE image; sample KR5329X1-4; peridotite (Finero Complex, Southern Alps, Italy).

Figure 9

Frequency distribution of grain boundary widths for Qz (a-d), Pl (e-f), Ol-Srp (g), and Ol (h). Sample numbers and numbers of measurements n are given. For sample KR5184X, one measurement of grain boundary width is outside the presented interval. The three arrows below each diagram indicate (from left to right) 25^{th} percentile, median, and 75^{th} percentile.

Figure 10

Relationship between (i) the angles of c-axes of pairs of Qz grains and the pole of the grain boundary between them and (ii) the width of the (open) grain boundary, exemplified by the samples KR4874 (left) and HH147B (right). The two angles α_1 and α_2 between the pole P of the grain boundary (double line) and the two Qz-c axes c_1 and c_2, as shown in the sketch, are added. They range between 0 and 180°. A low total angle indicates a grain boundary pole close to the c-axes of both grains; a high total angle points to a grain boundary pole close to the a-axes of both grains. Qz-c orientations and grain boundary poles were measured by universal stage.

Figure 11

Double-logarithmic plot of grain area versus width d of open grain boundary, based on SEM measurements of Qz as well as Pl, Ol and Srp from eight different samples with various P-T-deformation histories presented in figure 6. For each sample the 25^{th} and 75^{th} percentiles of grain boundary width d and grain area are presented (boxes) as well as median (circle), mean (+), the number of measurements n and the maximum temperature experienced by the sample. The samples KR2745A-1 and KR2745B-3x are from the same deformed pegmatite with flat, elongate, recrystallized Pl grains. The analyzed section of the first sample is cut perpendicular to the lineation and foliation (YZ section) (Fig. 2) and the section of the second sample parallel to the foliation (XY section) (Fig. 5e). Based on the measured areas and the X, Y, Z ratios taken from photomicrographs, the grain volumes are calculated and turned into cubes, the faces of which are taken as representative grain areas (Tab. 2).

Figure 12

Temperatures of opening of grain boundaries, based on the P-T paths of the analyzed samples and on contour lines of volume change. The latter represent the increase (or decrease) in % from the volume at 25 °C ('room temperature') and 1 bar to the volume at different P-T conditions. The P-T paths are taken from figure 6. **(a)** Temperatures of grain boundary opening of Qz for samples (1) HH147B, (2) KR4717, (3) KR4874, (4a) KR5184X and (4b) KR5185X. The contour lines (black solid lines) are based on data given by Raz et al. (2002, table 3). For each sample, additional contour lines are determined for the 25^{th} and 75^{th} percentile of measurements of grain area and the median of grain-boundary opening width (stippled lines in different colors) (Tab. 2), based on linear interpolation between the contour lines given by Raz et al. (2002). The two intersections of the 25^{th} and 75^{th} percentile contour lines with the P-T path (dots) are projected on the T-abscissa (broken lines), indicating the range of opening temperature. **(b)** Temperature of grain boundary opening of Ol (forsterite; sample KR5329X1) and Pl (low albite; samples KR2745A and B). The contour lines (black solid lines) are solely related to Ol and based on data given by Katzura et al. (2009 – table 1). Additional contour lines are determined for the 25^{th} and 75^{th} percentile of measurements of grain area and the mean of grain-boundary opening width (stippled lines) (Tab. 2), based on linear interpolation between the contour lines given by Katzura et al. (2009). The two intersections of the 25th and 75th percentile contour lines with the P-T path (dots) are projected on the T-abscissa. For Pl, P-T data related to the 25th and 75th percentile of measurements of the grain area and for the median of opening width of the grain boundary (Tab. 3) are taken from Benusa et al. (2005) and Stewart and Limbach (1967) and projected from the P-T path on the T-abscissa.

Table 1

Statistical data of the analyzed grain boundaries and grain areas, which form the basis for figures 9, 11 and 12; and table 2. Measurements of boundary widths (asterisks) between Ol (forsterite) and Srp are more numerous than those of grain areas.

Table 2:

Volume changes of grains in the analyzed samples, based on median values and 25th and 75th percentiles given in table 1. Based on the measured area A, the grain volume V0 is calculated as cube except for samples KR2745A und KR2745B where grains are modelled as elongate cuboids. The volumes of these cuboids are turned into cubes leading to the recalculated grain areas (cube faces), in order to harmonize the calculation of the volume increase for all samples. For an estimate of limits of error or range of data scatter refer to figures 4 and 11.

Table 3:

Unit-cell volume (pressure) and molar volume (temperature) of low albite as functions of pressure and temperature along the retrograde P-T path of samples KR2745A and B. Pairs of pressure and temperature are taken from the retrograde P-T path. Underlined = original data from Benusa et al. (2005) (pressure) and Stewart and Limbach (1967) (temperature); *italics* = data generated by linear interpolation; bold = P-T conditions determined from the measured volume change related to the 25th and 75th percentiles of grain area and boundary width given in table 2.

Authors' contributions:

J.H. Kruhl and W.W. Schmahl designed the study. TEM measurements were performed by R. Wirth and SEM measurements by E. Griesshaber and J.H. Kruhl. The latter conducted the u-stage measurements. All authors discussed the results and contributed to the manuscript.

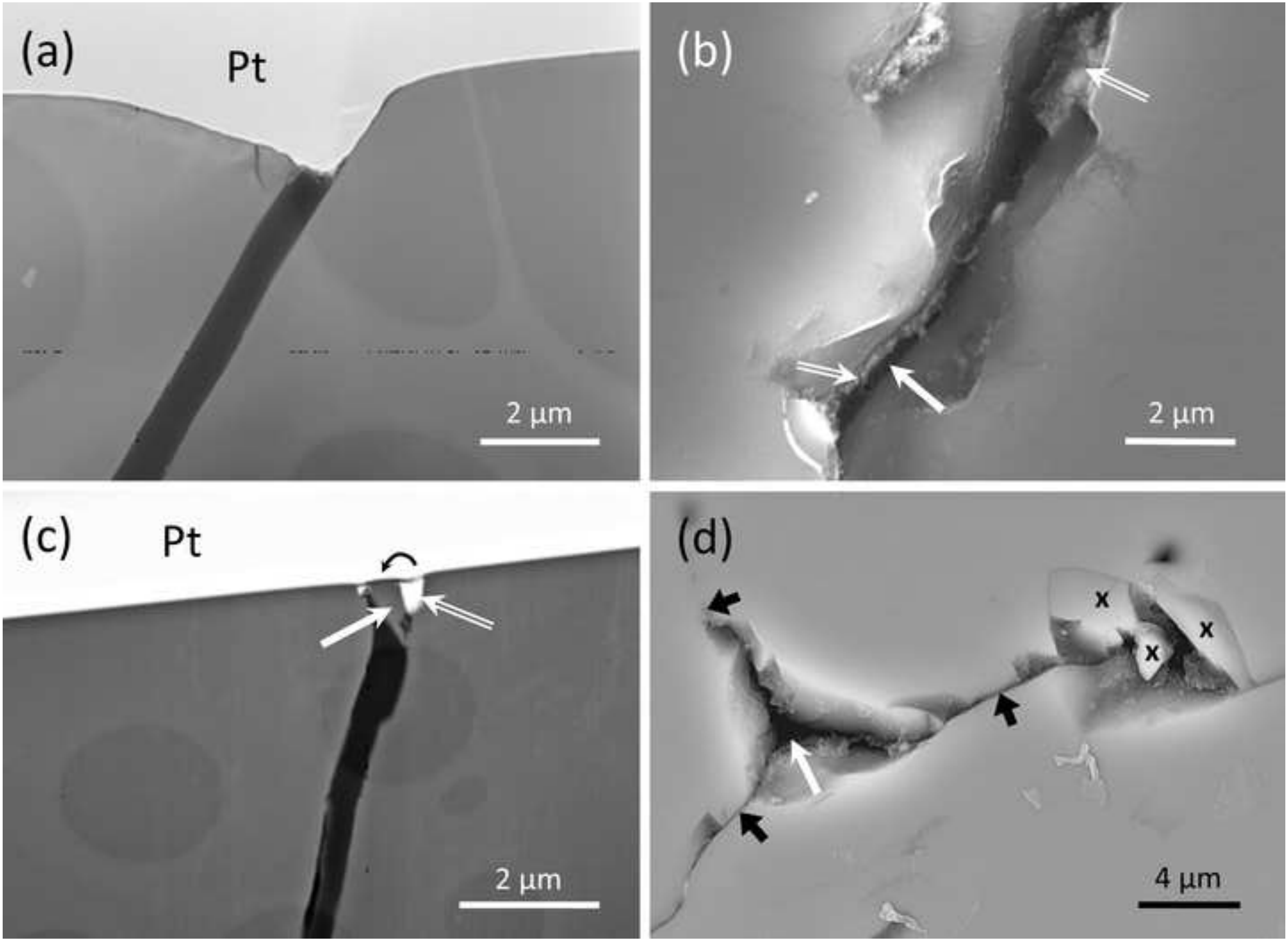
(a)
Pt
2 µm
(b)
2 µm
(c)
Pt
2 µm
(d)
x
x
x
4 µm

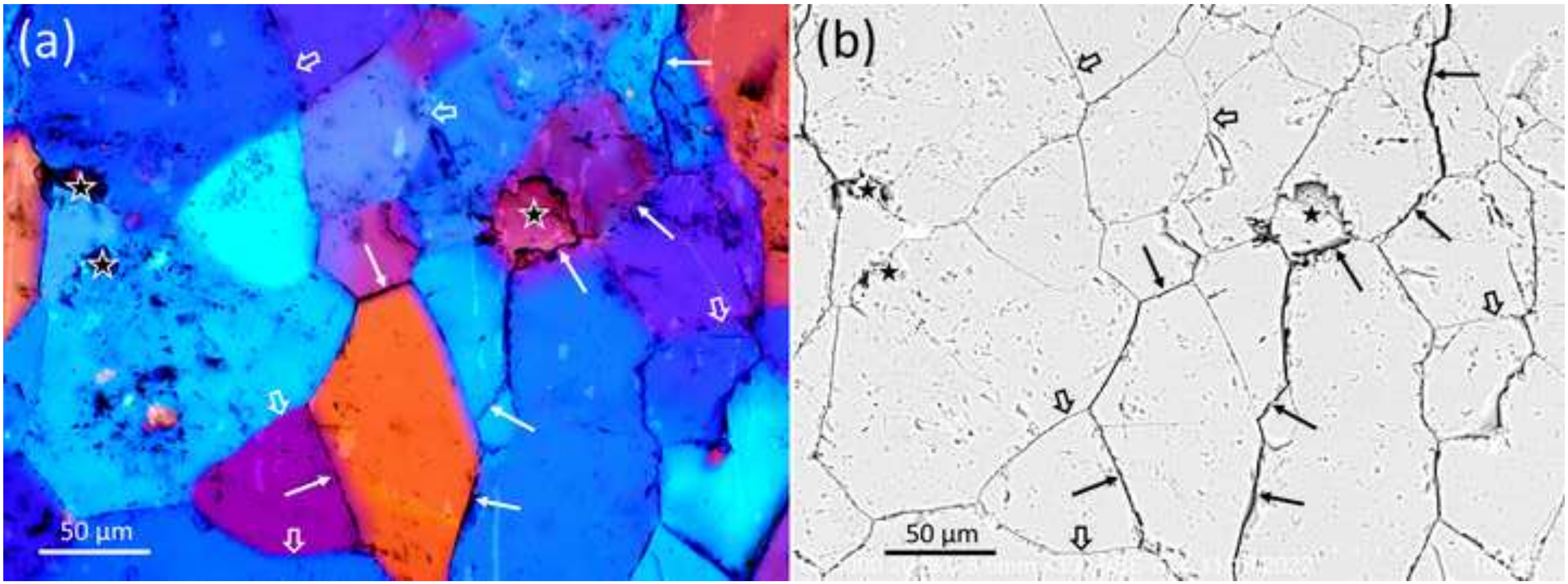
(a)
50 µm
(b)
50 µm

Figure_3

Click here to access/download;Figure;Kruhl_etal_Fig3_revised.tif

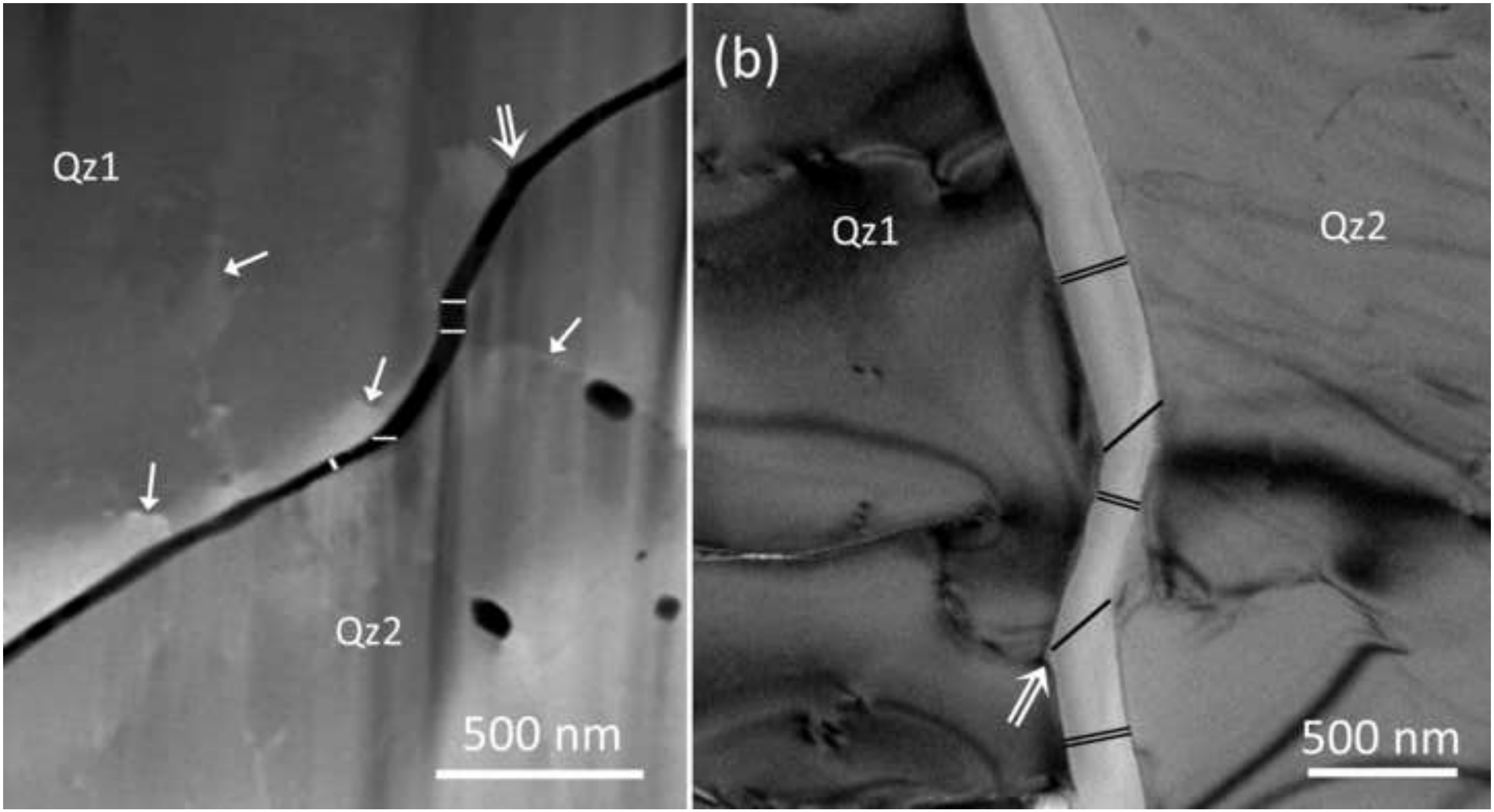

Figure_4

Click here to access/download;Figure;Figure_4.jpg

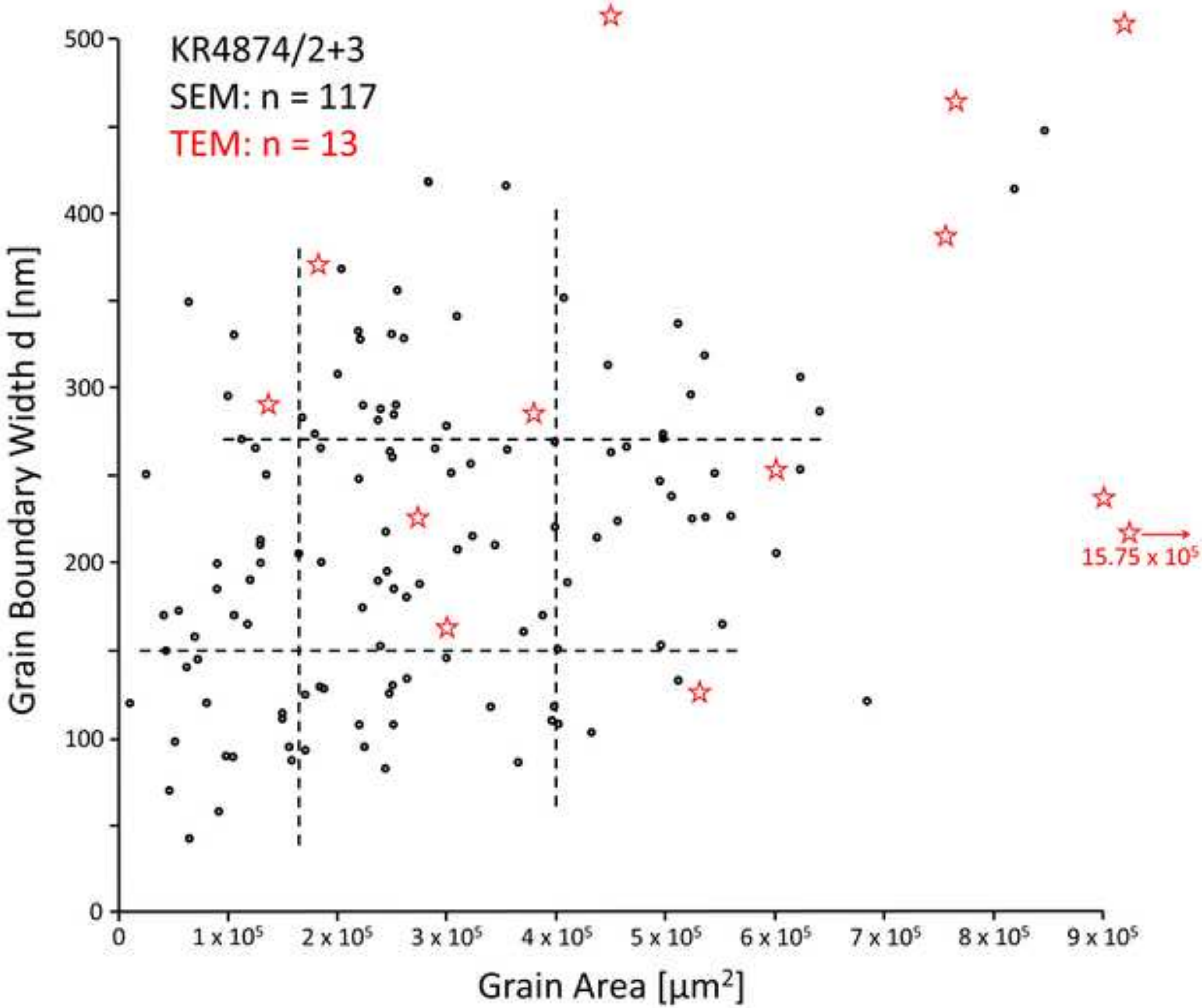

Figure_5

Click here to access/download;Figure;Figure_5.jpg

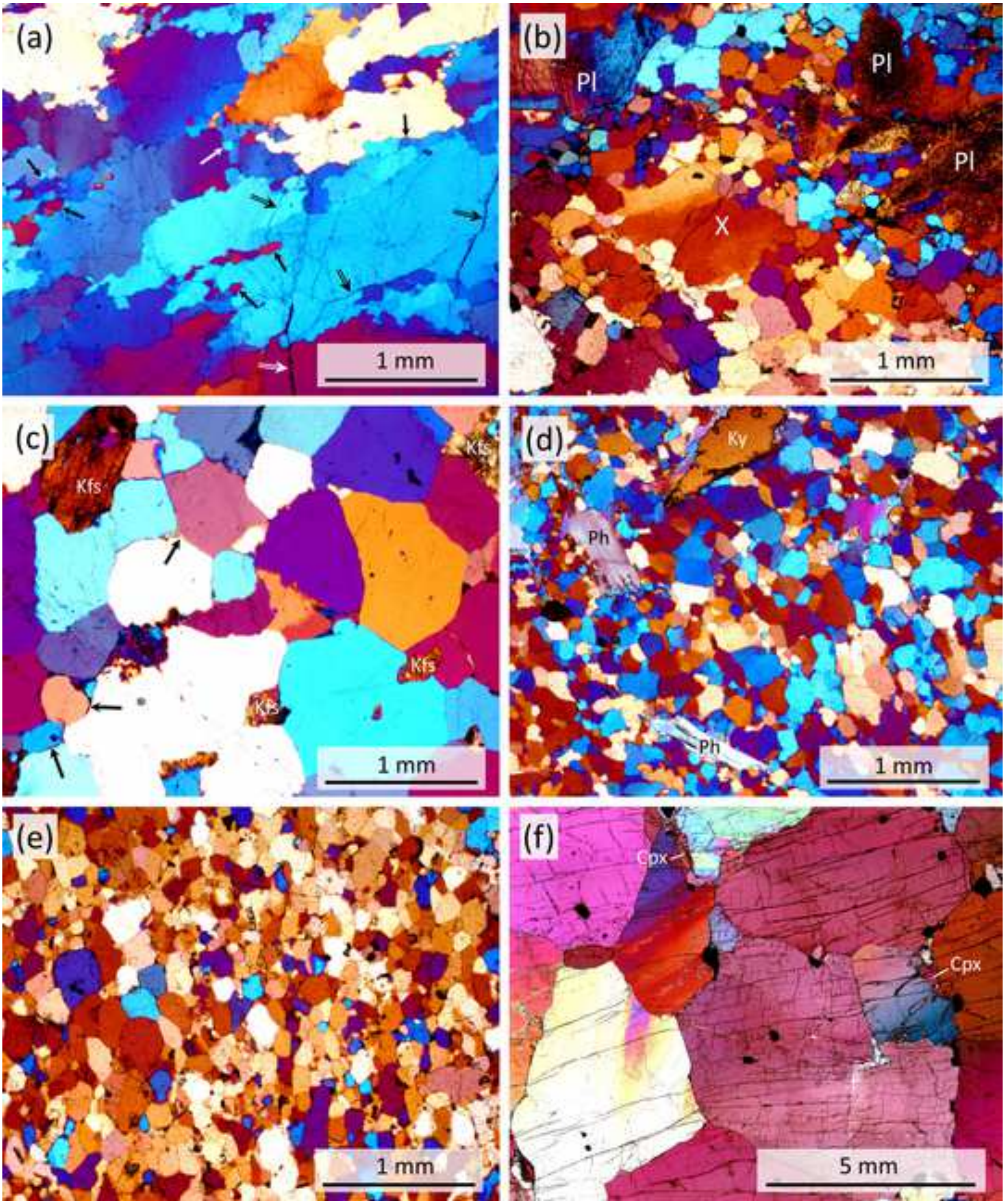

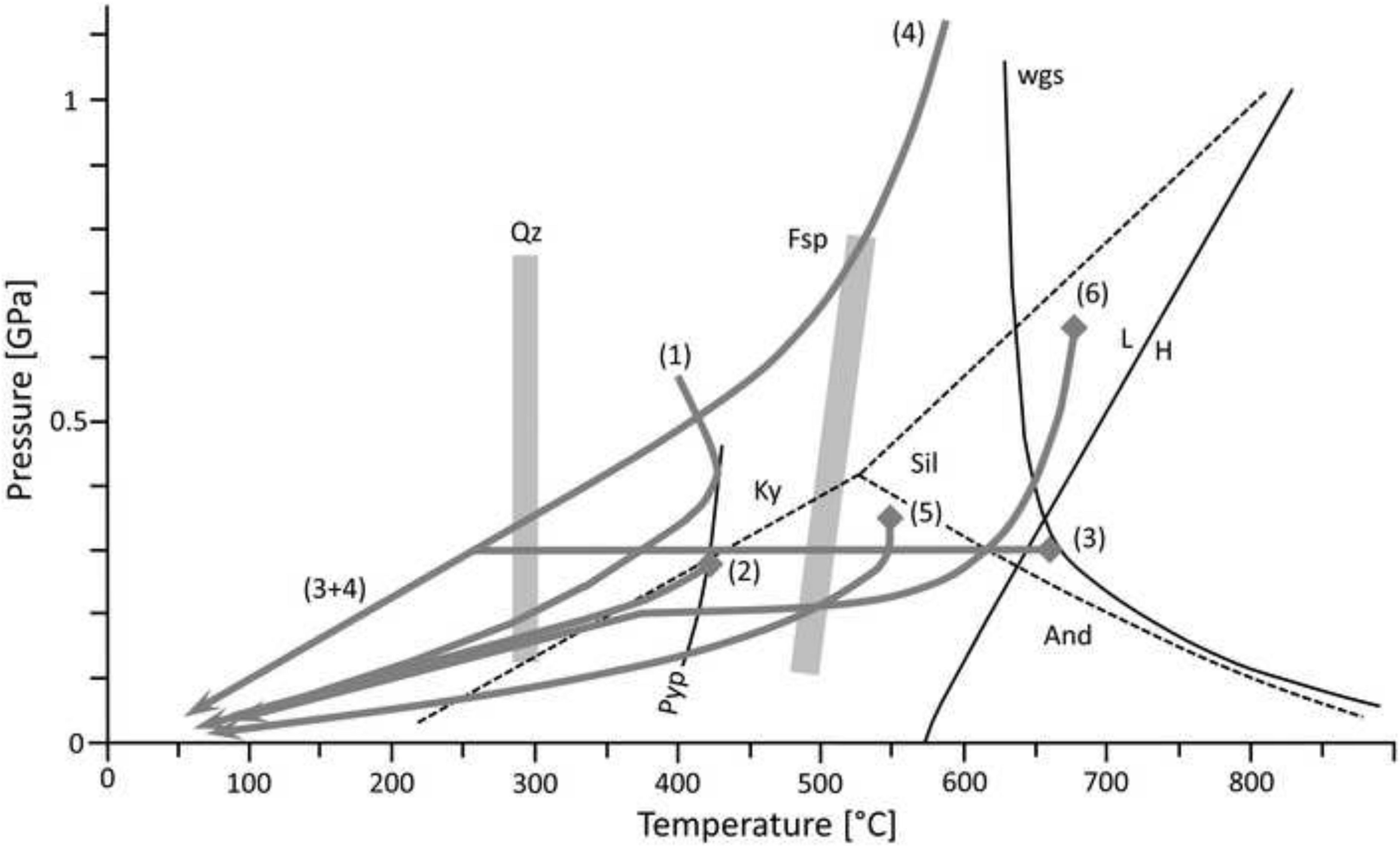
(4)
wgs
1
Qz
Fsp
(6)
L
H
(1)
0.5
Pressure [GPa]
Sil
Ky
(5)
(3)
(2)
(3+4)
And
Pyp
0
0
100
200
300
400
500
600
700
800
Temperature [°C]

Figure_7

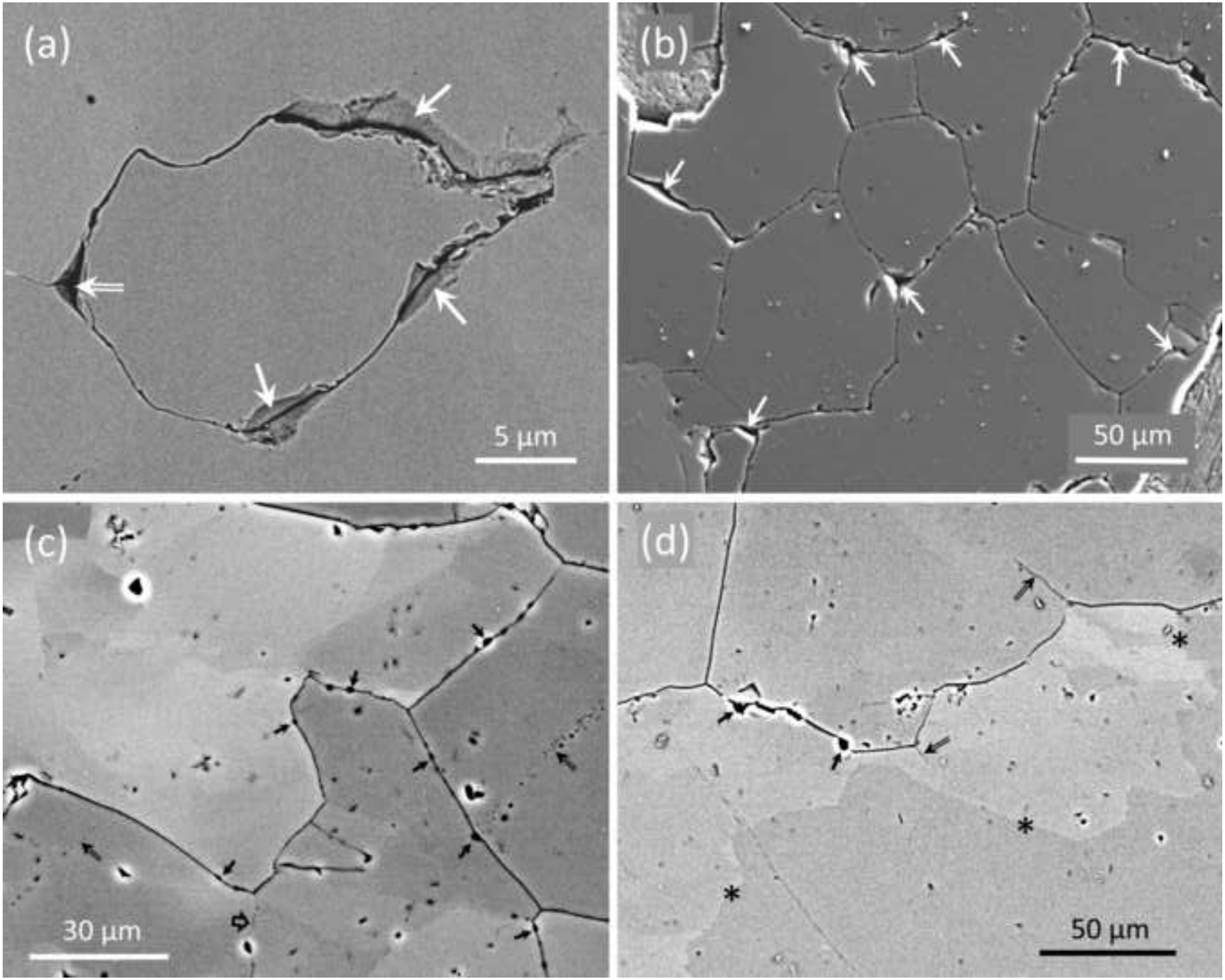

Figure_8

Click here to access/download;Figure;Figure_8.jpg

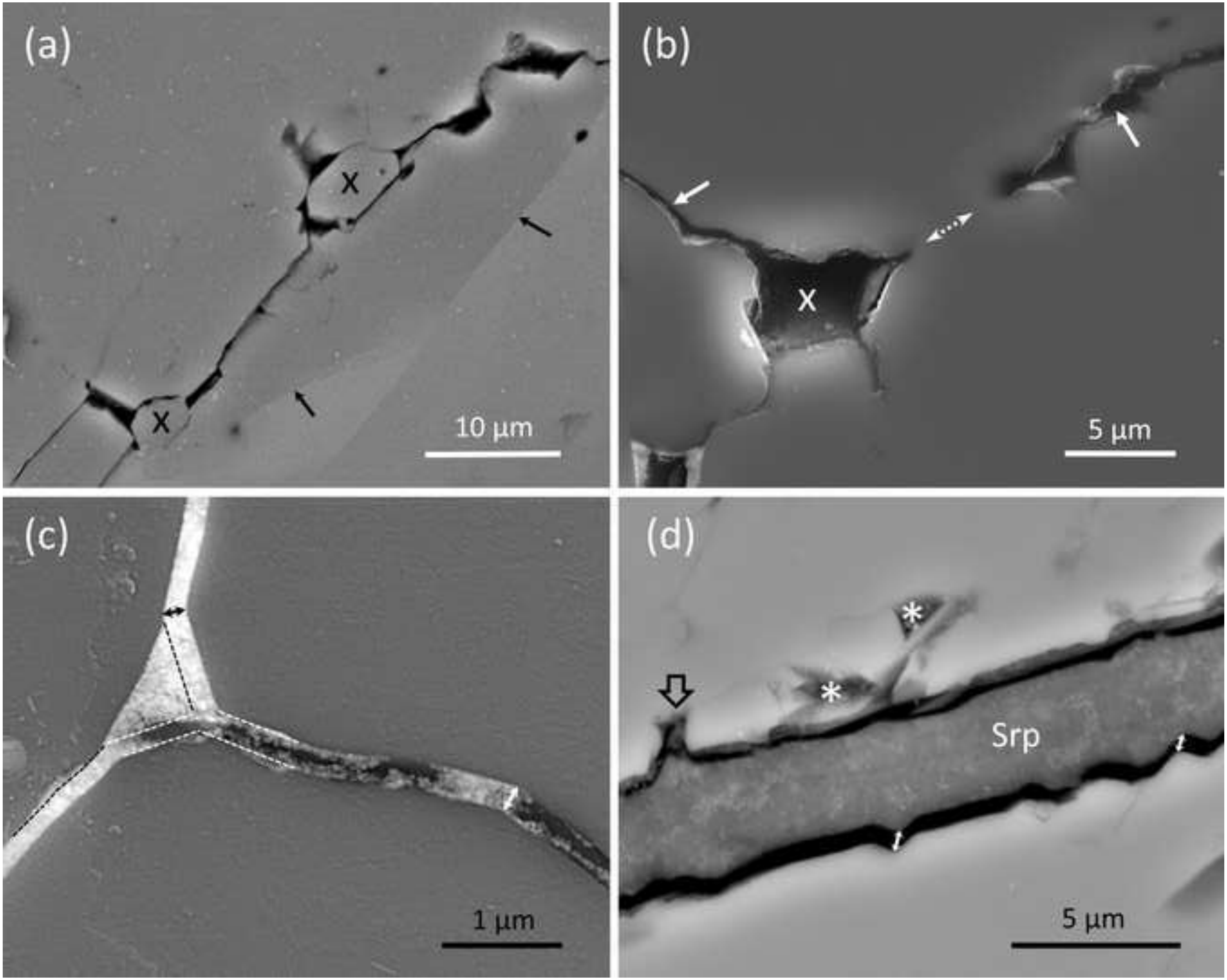

Figure_9

Click here to access/download;Figure;Kruhl_etal_Fig9_revised.jpg

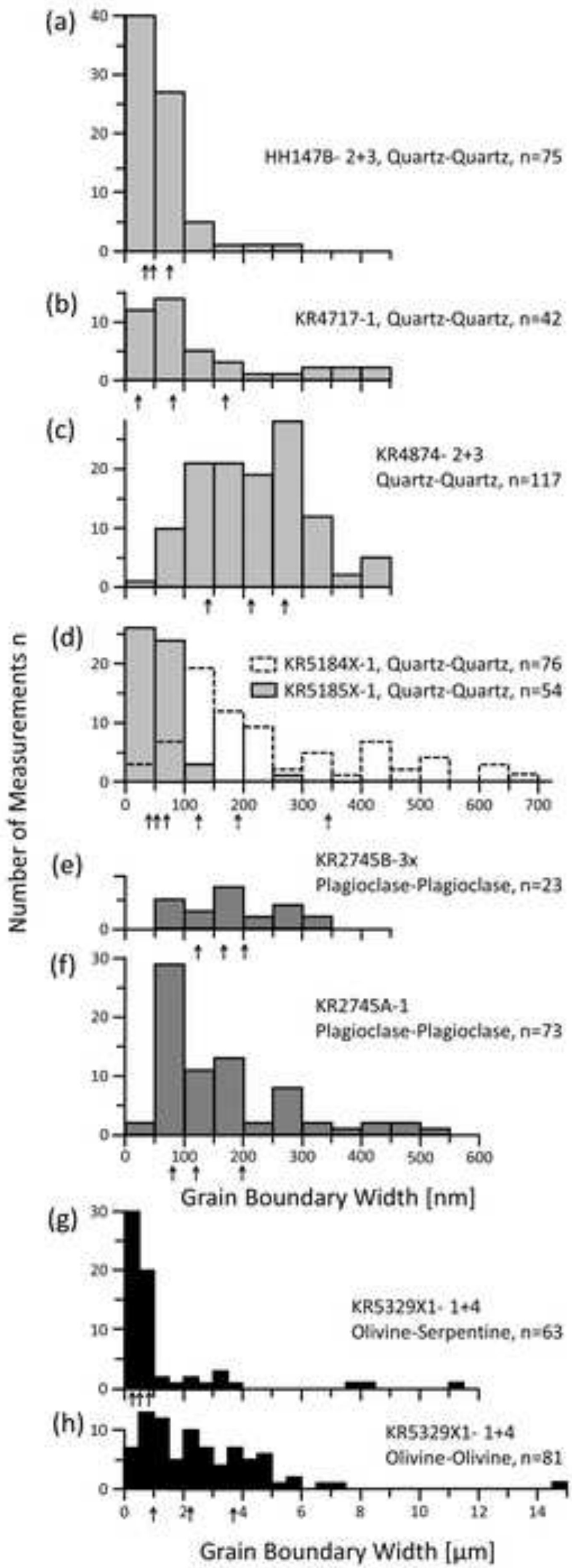

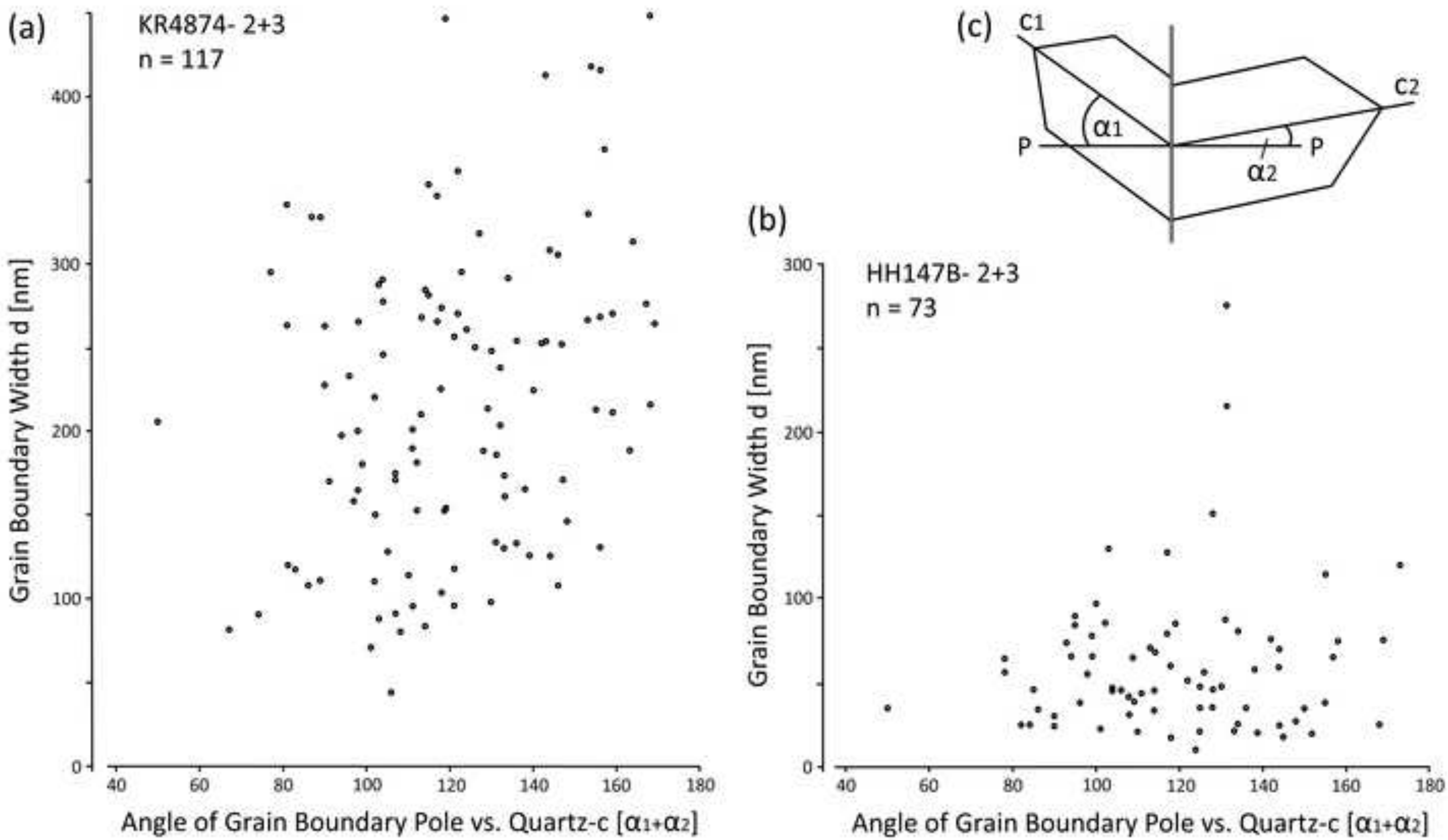
(a)
KR4874- 2+3
n = 117
Grain Boundary Width d [nm]
Angle of Grain Boundary Pole vs. Quartz-c [α1+α2]
(b)
HH147B- 2+3
n = 73
Grain Boundary Width d [nm]
Angle of Grain Boundary Pole vs. Quartz-c [α1+α2]
(c)
C1
C2
P
P
α1
α2

Figure_11

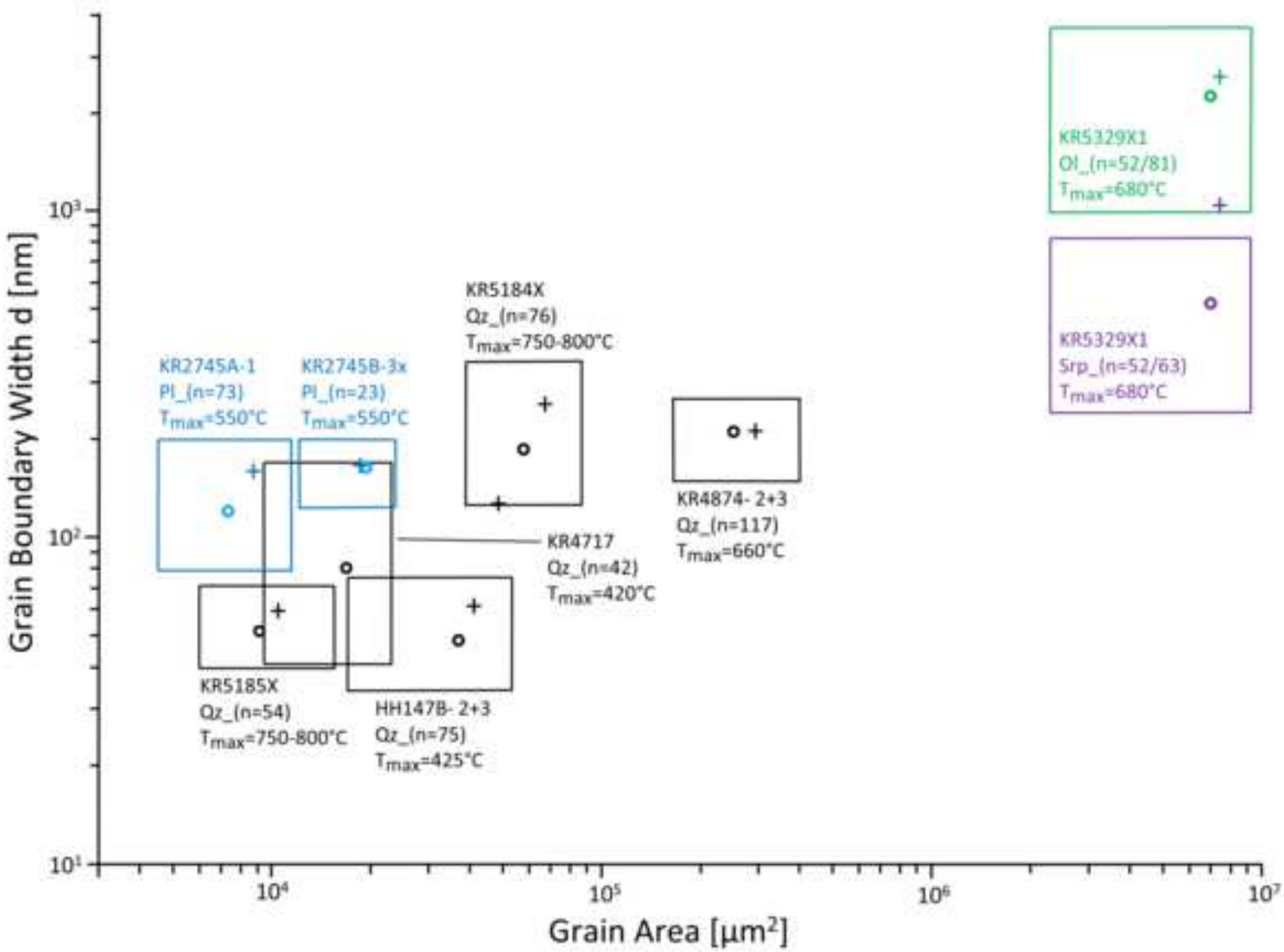
KR5329X1
Ol_(n=52/81)
Tmax=680°C
KR5329X1
Srp_(n=52/63)
Tmax=680°C
KR5184X
Qz_(n=76)
Tmax=750-800°C
KR2745A-1
Pl_(n=73)
Tmax=550°C
KR2745B-3x
Pl_(n=23)
Tmax=550°C
KR4874- 2+3
Qz_(n=117)
Tmax=660°C
KR4717
Qz_(n=42)
Tmax=420°C
KR5185X
Qz_(n=54)
Tmax=750-800°C
HH147B- 2+3
Qz_(n=75)
Tmax=425°C
Grain Boundary Width d [nm]
Grain Area [µm²]
10¹
10²
10³
10⁴
10⁵
10⁶
10⁷

Figure_12

Click here to access/download;Figure;Kruhl_etal_Fig12_revised.tif

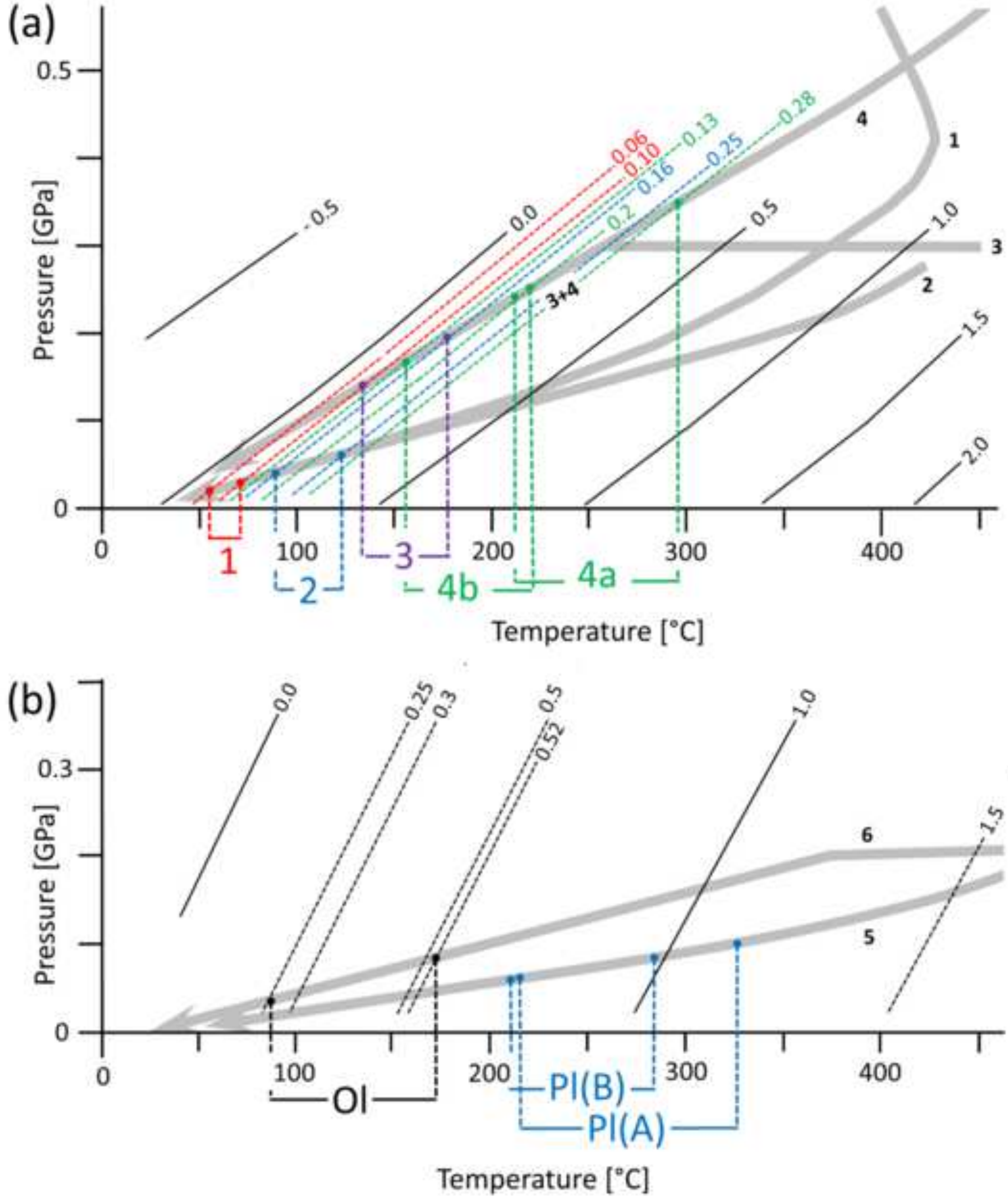

Table 1

Statistical data of the analyzed grain boundaries and grain areas, which form the basis for figures 9, 11 and 12, and Table 2. Measurements of boundary widths (asterisks) between olivine (forsterite) and serpentine are more numerous than those of grain areas.

Sample	Minerals	Measure-ments	Median / Mean of Grain-Boundary Width [nm]	25th / 75th Percentile of Grain-Boundary Width [nm]	Median / Mean of Grain Area [10^6 µm^2]	25th / 75th Percentile of Grain Area [10^6 µm^2]
HH147B- 2+3	Qz-Qz	75	48 / 61	34 / 76	0.037 / 0.042	0.017 / 0.054
KR4717-1	Qz-Qz	42	81 / 127	41 / 170	0.017 / 0.049	0.009 / 0.023
KR4874- 2+3	Qz-Qz	117	212 / 216	149 / 270	0.251 / 0.296	0.165 / 0.401
KR5184X-1	Qz-Qz	76	185 / 255	124 / 345	0.058 / 0.067	0.039 / 0.087
KR5185X-1	Qz-Qz	54	53 / 61	40 / 71	0.009 / 0.012	0.006 / 0.016
KR2745A-1	Pl-Pl (Ab)	73	120 / 162	79 / 198	0.006 / 0.007	0.004 / 0.009
KR2745B-3x	Pl-Pl (Ab)	23	167 / 166	124 / 201	0.026 / 0.025	0.016 / 0.031
KR5329X1- 1+4	Ol-Ol (Fo)	81*/ 52	2593 / 3431	1428 / 4868	7.125 / 7.435	2.278 / 9.263
KR5329X1- 1+4	Ol(Fo)-Srp	63*/ 52	523 / 1149	241 / 824	7.125 / 7.435	2.278 / 9.263
		604				

Table 2: Volume changes of grains in the analyzed samples, based on median values and 25th and 75th percentiles given in table 1. Based on the measured area A, the grain volume V0 is calculated as cube except for samples KR2745A und KR2745B where grains are modelled as elongate cuboids. The volumes of these cuboids are turned into cubes leading to the recalculated grain areas, in order to harmonize the calculation of the volume increase for all samples. For an estimate of limits of error or range of data scatter refer to Fig. 4 and 11.

Sample	Grain Boundary	n	Measured (Recalculated for cube-shape) Grain Area A [10^3 µm^2] given as Median m and 25th and 75th Percentile (p25 and p75)	Grain Volume V0 [10^6 µm^3]	Grain Boundary Width d [µm] (median)	Grain Volume Increase V1 = A x d / 2 x 6 at Elevated P-T Conditions [10^6 µm^3]	Volume Increase V1 (% of V0) from Ambient to Elevated P-T Conditions
(1) HH147B	Qz-Qz	75	m: 37.1 p25: 17.2 p75: 53.8	7.15 2.25 12.46	0.048	0.0054 0.0025 0.0077	0.0747 0.1010 0.0621
(2) KR4717	Qz-Qz	42	m: 16.8 p25: 9.4 p75: 23.0	2.17 0.91 3.48	0.081	0.0041 0.0023 0.0056	0.1876 0.2508 0.1604
(3) KR4874	Qz-Qz	117	m: 251.2 p25: 165.3 p75: 400.6	125.92 67.20 253.59	0.212	0.1598 0.1051 0.2548	0.1269 0.1564 0.1005
(4A) KR5184X	Qz-Qz	76	m: 57.7 p25: 38.9 p75: 87.5	13.86 7.67 25.88	0.185	0.0320 0.0216 0.0486	0.2309 0.2816 0.1878
(4B) KR5185X	Qz-Qz	54	m: 9.5 p25: 6.1 p75: 15.6	0.92 0.47 1.95	0.053	0.0015 0.0010 0.0025	0.1635 0.2040 0.1273
(5A) KR2745A	Pl-Pl	73	m: (7.4) p25: (4.6) p75: (11.5)	0.64 0.31 1.23	0.120	0.0027 0.0016 0.0041	0.4186 0.5309 0.3364
(5B) KR2745B-3x	Pl-Pl	23	m: (19.7) p25: (12.0) p75: (23.3)	2.76 1.31 3.57	0.167	0.0197 0.0120 0.0233	0.3572 0.4576 0.3278
(6) KR5329X1-1+4	Ol-Ol	81*/ 52	m: 7124.8 p25: 2278.9 p75: 9263.1	19,017.91 3,440.27 28,192.42	2.593	55.4241 17.7277 72.0574	0.2914 0.5153 0.2556

Table 3: Unit-cell volume (pressure) and molar volume (temperature) of low-albite as functions of pressure and temperature along the retrograde P-T path of samples KR2745A and B. Pairs of P and T are taken from the retrograde P-T path. Underlined = original data from Benusa et al. (2005) (pressure) and Stewart and Limbach (1967) (temperature); *italics* = data generated by linear interpolation; bold = P-T conditions determined from the measured volume change related to the 25th and 75th percentiles of grain area and boundary width given in table 2.

Pressure	**Unit Cell Volume**		**Temperature**	**Molar Volume**		
P [GPa]	**V [Å³]**	**dVP[%]**	**T [°C]**	**V [cm³/mol]**	**dVT[%]**	**dVT-dVP [%]**
0.001	664.760		26	100.062		
0.020		*-0.0363*	100	100.226	0.16	*0.1237*
0.035		*-0.0635*	150		*0.28*	*0.2165*
0.050		*-0.0907*	200	100.459	0.40	*0.3093*
0.054			**211**			**0.3278 (B)**
0.057			**216**			**0.3364 (A)**
0.070		*-0.1270*	250		*0.52*	*0.3930*
0.080			**285**			**0.4576 (B)**
0.085		*-0.1542*	300	100.705	0.64	*0.4858*
0.095			**327**			**0.5309 (A)**
0.105		*-0.1904*	350		*0.77*	*0.5796*
0.135		*-0.2449*	400	100.965	0.90	*0.6551*
			500	101.260	1.20	
0.200		*-0.3532*			*1.42*	*1.0668*
0.455	659.272	-0.8256				
			600	101.529	1.47	